SANDIA REPORT

SAND2004-6347
Unlimited Release
Printed December 2004

Compact Fuel Cell System Utilizing a Combination of Hydrogen Storage Materials for Optimized Performance

Jennifer P. Chan, Daniel E. Dedrick, Greg L. Ng, Karl J. Gross

Prepared by
Sandia National Laboratories
Albuquerque, New Mexico 87185 and Livermore, California 94550

Sandia is a multiprogram laboratory operated by Sandia Corporation,
a Lockheed Martin Company, for the United States Department of Energy's
National Nuclear Security Administration under Contract DE-AC04-94AL85000.

Issued by Sandia National Laboratories, operated for the United States Department of Energy by Sandia Corporation.

Available to DOE and DOE contractors from
U.S. Department of Energy
Office of Scientific and Technical Information
P.O. Box 62
Oak Ridge, TN 37831

Telephone: (865)576-8401
Facsimile: (865)576-5728
E-Mail: reports@adonis.osti.gov
Online ordering: http://www.osti.gov/bridge

Available to the public from
U.S. Department of Commerce
National Technical Information Service
5285 Port Royal Rd
Springfield, VA 22161

Telephone: (800)553-6847
Facsimile: (703)605-6900
E-Mail: orders@ntis.fedworld.gov
Online order: http://www.ntis.gov/help/ordermethods.asp?loc=7-4-0#online

SANDIA REPORT

SAND2004-6347
Unlimited Release
Printed December 2004

Compact Fuel Cell System Utilizing a Combination of Hydrogen Storage Materials for Optimized Performance

Jennifer P. Chan, Daniel E. Dedrick, Greg L. Ng, Karl J. Gross
Analytical Materials Science Department and the Microsystems & Advanced Concepts Engineering Department
Sandia National Laboratories
P.O. Box 969
Livermore, California 94551-9420

Abstract

An entirely new class of light-weight reversible hydrides was recently discovered (the Ti-doped alanates)[1]. These $NaAlH_4$-based materials have demonstrated reversible hydrogen storage capacities of up to 5 wt%, nearly 4 times the gravimetrically density of commercial metal hydrides. For this reason, they have been considered a breakthrough for hydrogen storage in fuel cell vehicles. This project is the first to publish the use of alanates for the generation of electrical power and the first demonstration of a hydride-fueled elevated-temperature PEM Fuel Cell. Because the kinetics of hydrogen uptake and release by the alanate improves with elevated temperatures, novel concepts were tested for the purpose of developing a highly efficient stand-alone power system. A major focus of this work was on the modeling, design, construction and testing of an integrated fuel cell stack and hydrogen storage system that eliminates the need of complicated heat transfer systems and media. After extensive modeling efforts, a proof-of-concept system was built that employs an integrated fuel cell stack and hydride beds that balancing the generation of fuel cell waste heat with the endothermic release of hydrogen from the alanates. Our demonstration unit was capable of greater than one hour of operation on a single charge of hydrogen from the integrated 173 gram alanate bed. In addition, composite hydride materials with synergistic reaction heats were evaluated and tested to enhance the operational performance of the alanates. The composites provide a unique opportunity to utilize the heat produced from hydriding classic metal hydrides to improve both absorption and desorption rates of the alanates. A particular focus of the mixed storage materials work was to balance the thermodynamics and kinetics of the hydrides for start-up conditions. Modeling of the sorption properties proved invaluable in evaluating the optimum composition of hydrides. The modeling efforts were followed by full validation by experimental measurements. This project successfully completed the proof-of-concept goals and generated a powerful set of tools for optimizing the complete power-generation system. It has also created a new direction for hydrogen power generation as well the potential for new R&D based on this work.

Acknowledgements

The authors would like to acknowledge Jens Oluf Jensen and the researchers at the Technical University of Denmark for supplying the prototype fuel cell that made this project so overwhelmingly successful. Acknowledgement is also given to Sandians Weifang Luo for her advice on materials, Terry Johnson for modeling of the single bed, Greg Roberts for commercial fuel cell selection, Ken Stewart and Steve Karim for their mechanical expertise, and Scott Spangler for materials preparation and analysis. Acknowledgements would be incomplete without recognizing Bill Replogle for his role in program management.

Contents

Figures

Tables

Nomenclature

OD	Outside Diameter
PBI	polybenzimidazole
PCT	Pressure Composition Temperature isotherm
PEM	Proton Exchange Membrane
PFSA	Perfluorosulfonic acid
THF	Tetrahydrofuran

1 Introduction

Nothing has so profoundly affected human existence as our relatively recently acquired ability to harness energy from fossil-fuel resources. It was this access to cheap and abundant energy that ignited the "Industrial Revolution" and continues to fuel rapid industrial expansion.

Today, on a worldwide average, each person consumes over 30 times more energy compared to their early agricultural ancestors of ten thousand years ago [1, 2 ,p.32, 3 p.77, 4 p.216]. Due to increasing personal energy consumption and an exploding population of energy consumers, average world-wide energy usage is skyrocketing (Figure 1). Mankind, as a whole, now consumes 10 times (60 times in the United States) the energy it did less than a century ago.

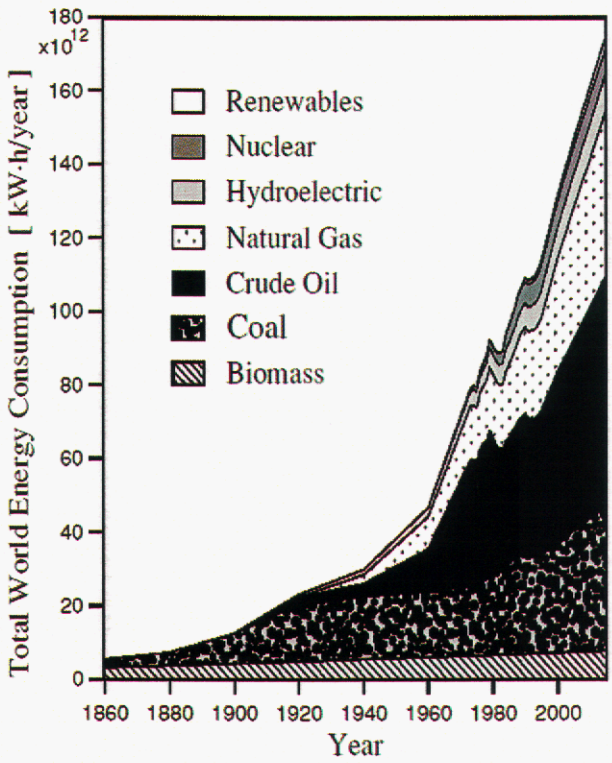

Figure 1. Total world energy consumption by source and projections to the year 2030 (assuming present rates of population growth and per capita energy consumption) [3 p. 77,5, 6].

Fuels for transportation are a particularly important component of the global energy system and economy. Today, worldwide transportation industries rely on petroleum exclusively, which has negative political, social, and environmental implications. In the United States alone nearly 17 million new cars are produced each year. Within this role of transportation fuel, hydrogen could be a superior alternative and it is believed that it will play an important role in the future energy markets [4,7,8,9]. Some of the advantages of hydrogen over other energy storage chemicals are as follows:

1) Hydrogen has the highest energy density of all combustion fuels (See Figure 2).
2) The supply of hydrogen is global in nature and is limited only by the supply of primary energy resources.
3) The utilization of hydrogen produces essentially no pollution.
4) Hydrogen can be produced from clean and renewable energy resources, such as solar, hydroelectric, wind-power, etc.
5) Hydrogen can be transported and stored with less environmental impact than petroleum.

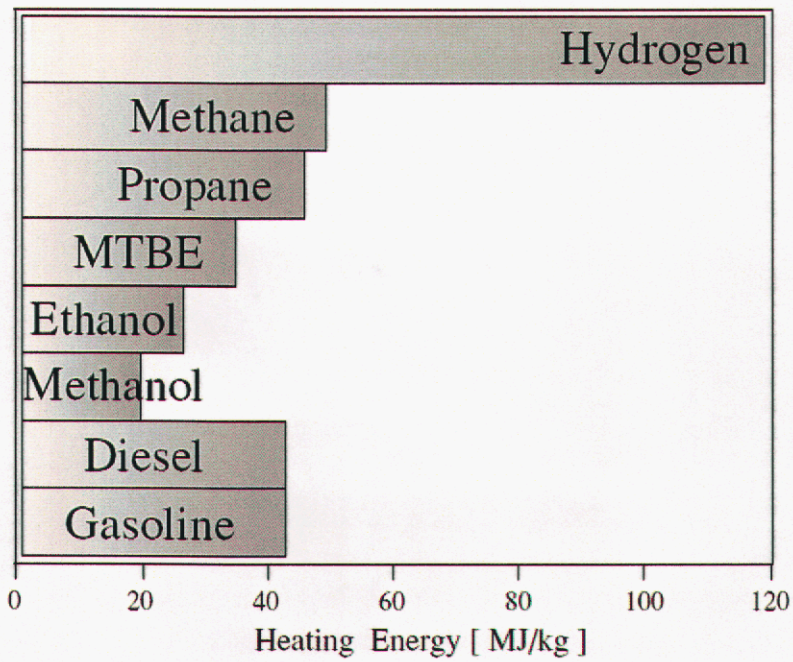

Figure 2. Heating-energy content by weight of several common fuels (MTBE: liquefied natural gas) [10p.50].

1.1 Hydrogen storage

Why are we not using hydrogen today?

One of the critical barriers to use of hydrogen as a primary energy carrier is the lack of a safe and practical means of hydrogen storage. Currently, hydrogen is stored and transported either as a gas under high pressure or as a cryogenic liquid at temperatures below 21 K. Gaseous hydrogen storage requires bulky and moderately heavy high-pressure vessels, whereas liquid hydrogen storage requires complex vacuum containment. Both methods are plagued by inefficiencies (the energy of compression and the energy of liquefaction and boil-off) and safety issues. Moreover, these methods of hydrogen storage cannot go beyond the bounds of hydrogen's physical properties as H2 gas or liquid. In essence, minimal storage efficiency improvements can be made to current optimized compressed or liquefied hydrogen storage systems available today.

The future of hydrogen storage and hydrogen energy in general lies in the development of advanced materials that can be used to more effectively store hydrogen through chemical bonding or physical sorption. An example of chemical hydrogen storage is the use of hydrides. Hydrides can store more hydrogen on a weight or volume basis than either compressed or liquid hydrogen (Figure 3). One subset of hydrides is the intermetallic compounds that have the ability to reversibly absorb and desorb large quantities of hydrogen. They have many advantages over the conventional methods of hydrogen storage. In particular, hydrogen may be stored at near ambient temperatures and pressures. These compounds can be stable enough to prevent accidental hydrogen release and provide high purity hydrogen gas due to the chemical sorption of impurities.

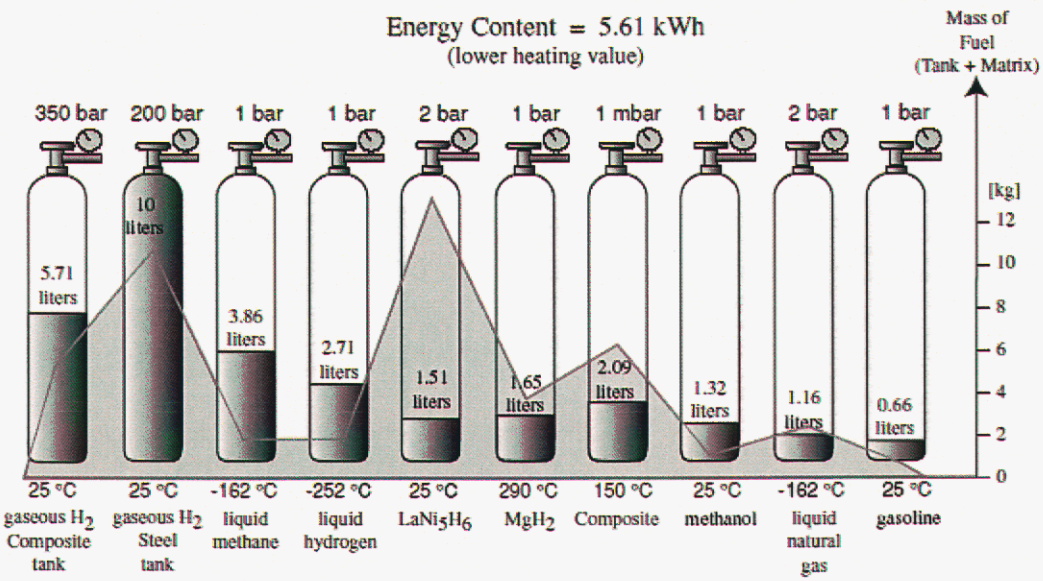

Figure 3. A comparison of the volumes and weights of different energy carriers based on an equivalent amount of stored energy.

Metal hydrides are commercially available today. Unfortunately, they are too heavy, too thermodynamically stable, or prohibitively expensive for most hydrogen storage applications. The development of superior metal hydrides is crucial for the successful transition to a hydrogen-powered economic structure.

1.2 Advanced hydrogen storage materials

Titanium-doped alanates offer an entirely new prospect for lightweight hydrogen storage. In 1996 Bogdanovic' and Schwickardi reported the break-through discovery that doping NaAlH4 with Ti-compounds enhanced reversible hydrogen uptake and release at moderate temperatures [11].

These materials have nearly ideal equilibrium thermodynamics [12,13]. Unlike the interstitial intermetallic hydrides, the alanates release hydrogen through a series of decomposition / recombination reactions:

$$NaAlH_4 \leftrightarrow 1/3Na_3AlH_6 + 2/3Al + H_2 \leftrightarrow NaH + Al + 3/2H_2 \qquad \text{(Eq.1)}$$

The two combined reactions give a theoretical reversible hydrogen storage capacity of 5.6 wt.%. However, the demonstrated state-of-the-art is closer to 4 wt.% H2 at reasonable charge and discharge rates.

Since the initial discovery of this new class of hydrogen storage materials much work has been done to understand the mechanisms of enhanced kinetics and to improve the hydrogen storage performance of the materials [14 - 19].

A number of new generations of materials with improved hydrogen storage properties were developed at Sandia National Laboratories. These include a dry-doping process of milling solid NaAlH4 (precipitated from THF) together with varying amounts of solid TiCl3. The first measurements on these materials were reported by Sandrock and co-workers [15,20]. Most recently we have developed solvent-free direct-synthesis methods in which Ti-dopants are milled directly together with NaH or Na and Al [21 - 23]. The current state-of-the-art performance for sodium-alanates is 3.6 wt% hydrogen uptake in 8 minutes at 100 °C with using a charging pressure of 100 bar. Hydrogen desorption is reported to reach 3.4 wt% released in 17 minutes at 150 °C against a pressure of < 0.5 bar [24].

1.3 Hydrides and heat requirements

The thermodynamics of metal hydrides can be best understood through the use of phase diagrams. Equilibrium metal-hydrogen phase diagrams are often constructed from Pressure Composition Temperature (PCT) measurements. These consist of isothermal measurements of the equilibrium hydrogen concentration in a metal as a function of the surrounding hydrogen gas pressure. An idealized representation of a PCT measurement is shown in Figure 4a.

Moving along one isotherm, hydrogen begins to dissolve into the host-metal lattice at low concentrations as the surrounding gaseous hydrogen pressure is increased. This is a solid solution of hydrogen in the metal that is generally denoted as the α phase. Hydrogen continues to be absorbed with increasing pressure until H-H interactions become important. At this point (1 in Figure 4a), a hydride (denoted β phase) is formed locally by the occupation of particular interstitial lattice sites. The nucleation and growth of the hydride phase may occur at free surfaces, at inter-grain boundaries, or throughout the bulk of the metal, depending on nucleation and diffusion mechanisms. Under idealized equilibrium conditions, the hydrogen gas pressure remains constant as hydrogen is absorbed and the α phase is transformed into the β phase. This is observed as a plateau in the PCT diagram.

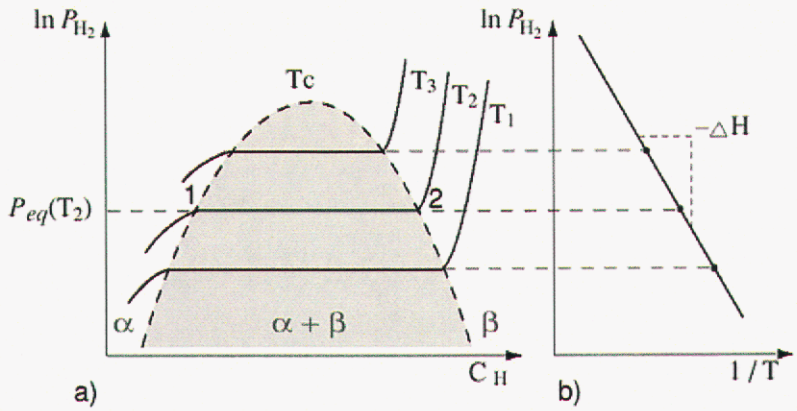

Figure 4. a) An idealized representation of Pressure Composition Temperature (PCT) isotherms for the α solid solution phase and β hydride phase. b) The enthalpy of hydride formation β H is obtained from the slope of a van't Hoff plot of ln(peq) versus 1/T.

The existence of an equilibrium plateau signals the co-existence of the two phases. As the hydride phase grows the sample's total hydrogen content increases. Eventually all of the α phase is transformed into the β hydride phase (point 2 in Figure 4a). The pressure again rises and the overall hydrogen concentration continues to increase as hydrogen is dissolved as a solid solution in the β hydride phase. The slope and length of the equilibrium plateau is of particular importance for hydrogen storage applications.

A flat plateau enables the reversible sorption of hydrogen from a metal simply by raising or lowering the surrounding hydrogen pressure above or below the plateau pressure. In raising the pressure, hydrogen is absorbed forming the hydride phase. Hydrogen is desorbed by lowering the pressure transforming the hydride back into the metal phase. This change in pressure can be minor (1 to 2 bar for the classic alloy LaNi5 at 22°C) compared to the pressures needed to store a significant amount of hydrogen by pressurization (350 bar). The length of the plateau determines how much hydrogen can be reversibly stored in a metal hydride.

Hydrogen absorption and release from complex hydrides such as the sodium-alanates displays similar PCT behavior. The reactions of equation 1 are in equilibrium with respect to gaseous hydrogen at specific temperatures and pressures. If the pressure is lowered or the temperature increased, the reactions will proceed to the right, releasing hydrogen by the decomposition of the hydride. If the pressure is raised or the temperature decreased, the reactions will proceed to the left, taking-up hydrogen by the formation of the hydride. Again, a plateau pressure can be observed in PCT measurements corresponding to the coexistence of the hydride and decomposition phases. Unlike interstitial hydrides, however, these reactions are characterized by very little solubility of hydrogen in hydride or decomposition phases. More importantly, in these "decomposition/reformation' compounds, uptake and release of hydrogen occurs through a complete change of chemical composition and crystal structure that may involve solid-solid as well as solid-gas reactions.

The ease with which hydrogen can be reversibly absorbed and desorbed depends on mass transport and the relative thermodynamic stability of the hydride with respect to the desorbed state. The formation of hydride phases is exothermic during absorption and endothermic during decomposition. The enthalpy of formation defines a phase's relative stability. This can be determined directly from a series of equilibrium PCT measurements at different temperatures as shown in Figure 5. Such measurements are critical to determining the practical hydrogen storage properties of new materials.

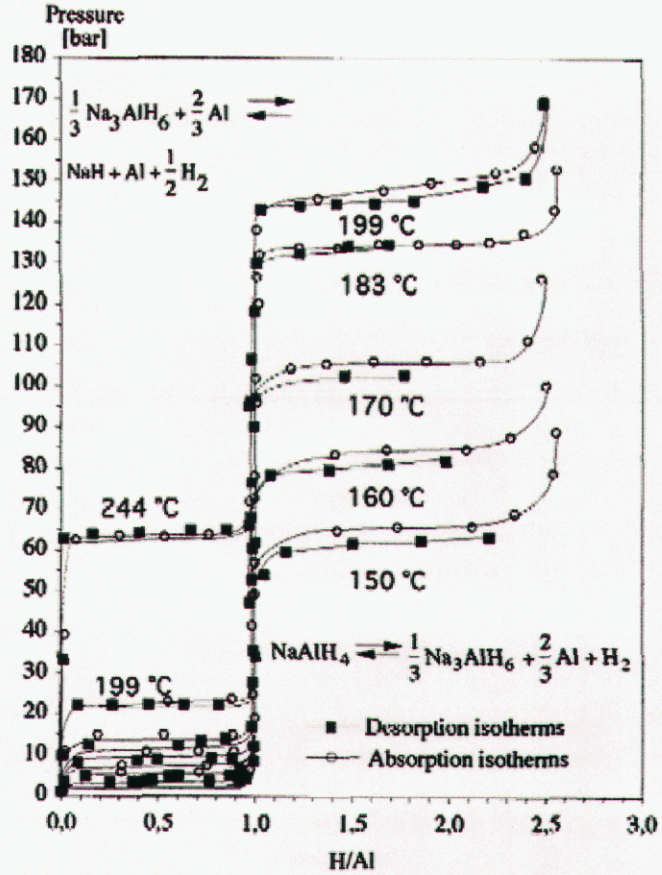

Figure 5. Hydrogen absorption and desorption measurements from sodium-alanates showing two reaction steps according to eq.1 [25].

The presence of two or more phases in equilibrium with hydrogen gas must satisfy the condition of balanced chemical potentials (equation 2).

$$\frac{1}{2}\mu_g(p,T) = \mu_\alpha(p,T,x) = \mu_\beta(p,T,x) \qquad \text{(Eq.2)}$$

$$\ln\left(\frac{p_{eq}}{p_o}\right)\Bigg|_T = -\frac{\Delta H^{\alpha\to\beta}}{RT}\Bigg|_T + \frac{\Delta S^{\alpha\to\beta}}{R}\Bigg|_T \qquad \text{(Eq.3)}$$

This leads to the van't Hoff relationship for the equilibrium pressure p_{eq}(T) in terms of the enthalpy , entropy and normal pressure p_o of the phase transition (equation 3). This relationship holds over a much larger temperature range than that commonly found in most applications (200 to 1000 K). Hence the transition enthalpy and entropy may be determined experimentally from the slope and intercept of a van't Hoff plot of ln(P_{eq}) versus 1/T.

Because the main contribution to the entropy is due to hydrogen in the gas phase, ΔS (the van't Hoff intercept) is fairly constant at 120 J/K•mol H2). Thus, to have an equilibrium sorption pressure of 1 bar at room temperature most materials will need reaction enthapy ΔH (the van't Hoff slope) of about 35kJ/molH2) this is equivalent to 14% of the lower heating energy for the oxidation of hydrogen. For automotive applications, as much as 5 kilograms of hydrogen must be stored onboard the vehicle. The heat required to release hydrogen from a room-temperature reversible hydride is 24.3 kW•hours of energy. This heat can generally be provided by the waste heat of the energy conversion device. For example, fuel cells are typically 40 to 50% efficient. Thus, 50 to 60% of the hydrogen energy is converted to heat which is more than sufficient to satisfy the 14% hydrogen desorption energy requirement of the hydride. The obstacle however, is that this heat may be at a temperature that is too low to be useful for desorbing the hydride.

Alanates, may have thermodynamics that allow for the delivery of hydrogen at ambient conditions, unfortunately the reaction kinetics are extremely slow at these temperatures. This is likely due to the intrinsic nature of these "decomposition / reformation" hydrides. The absorption and release of hydrogen not only involves making and breaking hydrogen-metal bonds but also involves changes in the metal structures and stoichiometries. Completely new compounds are formed and decomposed in the process, requiring long-range diffusion of metal species as well as hydrogen. This metal atom transport may be in the solid or local transport of gaseous species such as alanates. In any case, this extra transport process is probably much slower than hydrogen diffusion in interstitial hydrides and highly dependent on temperature. This behavior is likely to be characteristic of all "decomposition / reformation" hydrides. So, while it may be possible to develop improved catalysts and nano-material, low-temperature

operation may not be attainable with this general class of materials. To take advantage of these materials with their high hydrogen capacities, novel approaches to power system design will be required.

For reasonable reaction rates the alanates require working temperatures well in excess of 100°C. This is much higher than the 60 to 80°C waste heat temperatures of current PEM fuel cell technologies.

The second and more potentially more problematic issue is the recharging of reversible hydrides with hydrogen. To fully charge a 5kg hydride system in 5 minutes requires the removal of 300 kW of average thermal power. Thus, heat transfer is one of the most critical problems of reversible onboard hydrogen storage. Again, new approaches to heat transfer will be important for the advancement of these mobile power applications.

1.4 Project goals

Thermal management in most fuel cell systems using hydrides typically relies on heat exchangers using a liquid medium such as water or oil to provide the necessary heat transfer. This presents several problems. First, the pumping and regulation of the heat transfer fluid adds complexities such as heat transfer tubing in the hydride beds, pumps, valves, sensors and controls. This adds considerable weight, volume, complexity, cost and energy penalties to the system. Second, fluids such as water can be corrosive to the fuel cell and hydride bed container materials, and is also highly reactive with many hydrides.

To realize the potential advantages that fuel cell systems offer, one or more of the following problems must be solved. First, the heat flow to and from hydrogen-storage materials should be sufficient to meet the hydrogen uptake and delivery requirements. Second, fuel cell and the hydrogen-storage material temperatures should be maintained at levels that deliver optimum performance. Third, the hydrogen-storage unit should be economical and require less ancillary components and support systems than those of current fuel cell / hydrogen storage systems.

The following tasks were outlined for this project based on the overall goal of testing novel concepts for creating a simple and efficient light-weight power system based on a combination of a PEM fuel cell stack for chemical energy conversion and alanates for hydrogen storage.

1) ***Novel integrated approach to system thermal balance.***
A unique engineering design based on direct heat transfer from the fuel cell stacks to the hydride storage beds was envisioned for an autonomous power delivery system. A schematic diagram of this concept is shown in Figure 6.

The final test system design consisted of a fuel cell stack (6 cells) sandwiched between two hydrogen storage beds. The beds were designed to contain a maximum amount of alanate hydrogen storage material while withstanding charging pressures in excess of 100 bar and maintaining efficient direct-thermal contact with the fuel cell stack. Ultimately, data generated from this single stack system provides the basis for the design of a multiple fuel cell stack / hydride-bed power system with an unlimited number of different possible configurations. Some of the practical advantages of this concept are:

a) Modules of the system could be quickly exchanged for charged units

b) Repairs or power capability expansion could be simplified

c) Economic redundancy in a larger multi-unit power system (the entire power system, for example in a vehicle will not go down if one unit fails as is the case with a single fuel cell stack if one cell fails)

d) Optimum use of volume by employing multiple power-packs to take advantage of non-uniform spaces (in a vehicle for example)

e) Finally, a gain in simplicity and economy of scale by reducing the size and increasing the number of the individual unit.

Through modeling we evaluated and down-selected an advanced design utilizing integrated hydride-fuel cell stack. This would be the first system demonstrations based on novel hydride-fuel cell integration options to achieve an optimized power-pack. The selected design was ultimately constructed to demonstrate the concept and validate the modeling.

2) ***Modeling of heat and power generation for a typical demand cycle.***
Initial work focused on balancing the thermodynamics of the hydrides with start-up conditions. Modeling of the power demand cycles for typical applications was investigated as an initial step to determine an appropriate size of the demonstration system. A commercial fuel cell (Ballard AirGen 1000 Watts) was purchased, tested and modeled. This modeling helped to define the operable pressure and temperature ranges of the hydrogen storage materials as well as the waste heat requirements to provide a steady generation of hydrogen.

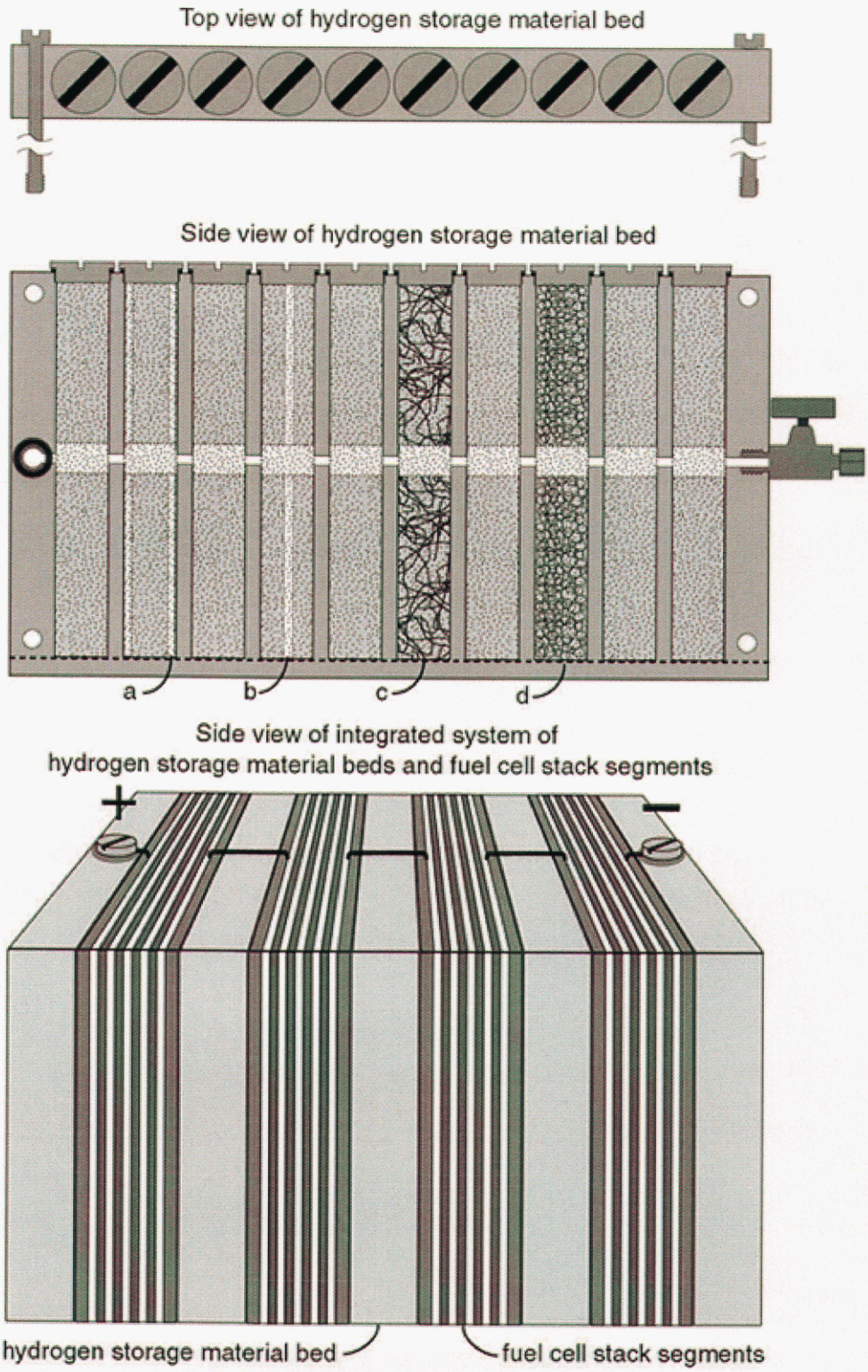

Figure 6. A schematic diagram of the basic integrated fuel cell / hydride bed concept. a,b,c, and d being different option of packing and construction of individual cell in the bed.

3) ***Composite hydrides for cold start-up.***
This study addresses the poor kinetics of alanates at room temperature. For cold-start conditions, a composite storage system of alanates and classic hydrides were used to readily enable delivery of hydrogen at room temperature. The Sandia database of the thermodynamic properties of classic hydrides [26] was used to evaluate and select the best interstitial hydride to be used in combination with the Alanates. Absorption and desorption rates were measured for the composite materials. This data, combined with the thermodynamic data from the second task, was incorporated into a model of the hydride kinetics and thermodynamics and used to select the optimal composition of hydrides.

4) ***Kinetics designed for rapid fill.***
The kinetics of hydrogen absorption into metal hydrides improves at elevated temperatures. The composite hydride design provides a unique opportunity to utilize the reaction heat produced by hydriding the interstitial metal hydrides to enhance the absorption rates of the alanates. It was thought that designing a synergistic match between the thermodynamic and kinetic properties of the component hydrides should dramatically reduce the hydrogen fill times. Once again, modeling thermal transport and hydride compositions was utilized to develop an understanding and a predictive capability this system. Experimental work confirmed that the recharging rate could be enhanced by using the two materials. This was true only when the materials are in separate gas handling sections of the same bed. This allows necessary heat transfer while maintaining control of the charge state of each material independently.

5) ***Hydrogen power milestone.***
The final demonstration product was a small stand-alone power pack consisting of a fully integrated set of the composite alanate-hydride beds and a fuel cell stack (Figure 7). Modeling demonstrated the need to have a fuel cell system that operated at higher temperatures than the traditional PEM fuel cells. A fully tested and operational High-Temperature PEM fuel cell was provided to us through a very helpful and beneficial collaboration with Jens O. Jensen, of the Materials Science Group in the Department of Chemistry, of the Technical University of Denmark. This fuel cell was tested at Sandia and our integrated bed was designed and constructed to work with specifically with this fuel cell for the demonstration tests. Its high operating temperature range of 150 – 200 °C is ideally matched to the hydrogen delivery performance of the alanates.

This test unit was designed for and is available to test more advanced complex hydrides, amides and other hydrogen storage materials as they become available. To our knowledge this is the first demonstration of electrical power generation from alanate hydrogen storage materials.

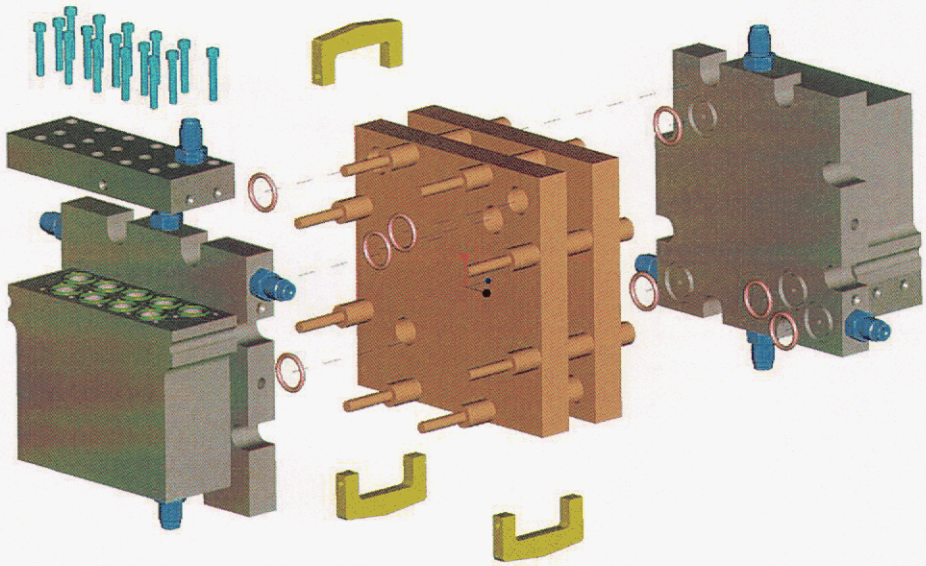

Figure 7. Solid model of final storage bed and fuel cell integration

2 Individual system component investigations

Prior to designing the fully integrated hydrogen storage and fuel cell system, individual component investigations were performed.

1. A state-of-the-art PEM fuel cell was purchased and tested to determine the operational characteristics. This data was valuable for the design of a system that matches the energy from the fuel cells with the thermodynamics and kinetics of the storage materials.
2. For stack startup conditions, combinations of hydrides with different thermodynamic and kinetic properties were selected based on operational limits of the fuel cell.
3. Proof-of-concept storage beds were built and tested using simulated fuel cell stack heat inputs.

The results of these efforts gave us the necessary tools to build a fully integrated and optimized fuel cell / hydrogen storage system.

2.1 Fuel cell selection and testing

Four fuel cell vendors were contacted to provide a fuel cell stack for this project (BCS Fuel Cells, Electronchem, Schatz/Humbodt University and H2 ECOnomy). During these communications, we also inquired regarding the availability of a customized stack for our final integrated system. All vendors were eager to provide us with a stack. However, the cost for a 300W stack is in order of $10k. A more economical solution presented itself as the commercially available Airgen™, a 1-Kilowatt fuel cell system produced by Ballard Fuel cells and distributed by Colman. The Airgen™ was sold as a fully packaged system including all control systems but no hydrogen storage. As an initial demonstration, the Airgen™ was utilized as a power source for a PCT materials research apparatus while supplied with hydrogen from C15 classic metal hydride beds designed and built by Sandia National Laboratories (Figure 8).

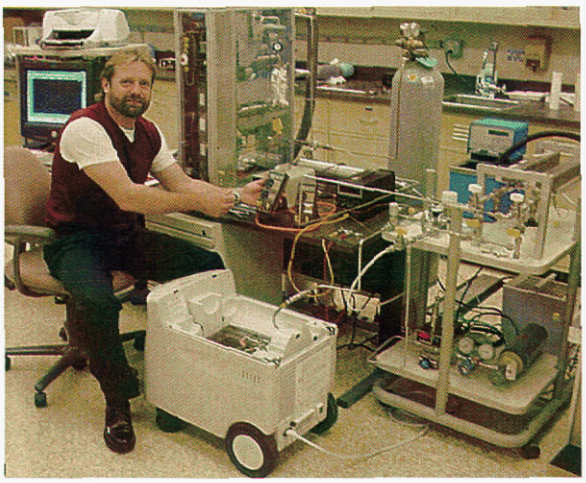

Figure 8. Airgen powering PCT station

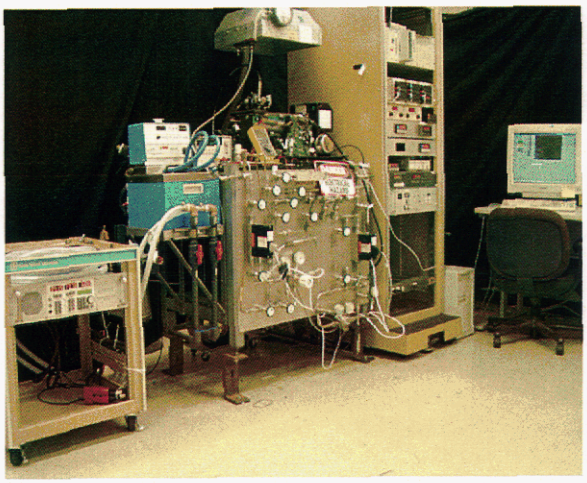

Figure 9. Nexa test bench apparatus

The Ballard Nexa™ stack is utilized in the Airgen™ fuel cell system. To characterize the performance and operational parameters of this system, we developed instrumentation that allowed us to measure:

- stack power output
- hydrogen consumption rate under various loads
- performance at lower, normal range and upper temperature limits
- heat dissipated from the stack

The completed system employed the Nexa fuel cell installation kit, a LABVIEW™ controlled data acquisition system, and a custom-built hydride manifold (Figure 9). The data acquisition system collected temperature, voltage, current, and fuel consumption data. A schematic of the test apparatus is shown in the Appendix, Figure 35.

Experiments were completed to evaluate thermal-energetic characteristics of the Nexa 1kW fuel cell system. The efficiency of the stack can be calculated based on a ratio of energy produced to the total energy expected from the oxidation of hydrogen (lower heating value, 119.6 KJ/g). The efficiency of the system was measured for various operational loads, ranging from 25W to the maximum 1.2 kW. Fuel consumption included the hydrogen purge cycle, since purges are a necessary function of the system operation. Peak efficiencies exceeded 50% while maximum net power was measured at over 1.2 kW at a peak hydrogen flow rate of 17 slpm (results are plotted in Figure 10). Results from this testing were utilized to calculate the quantity of hydride materials needed for storage bed integration and to determine the amount of exhaust heat available from the fuel cell. The stack required approximately 10 minutes to reach an operating temperature of 50 °C from room temperature at various operational loads. This time is defined as warm-up time.

In the final assessment, it was determined that the development of advanced alanate materials have not progressed to the point that a standard PEM fuel cell can provide waste heat at high enough temperatures to promote sufficient kinetic performance. For this reason we determined that it would be necessary to use a higher-temperature PEM for the final demonstration tests. High-temperature PEM stacks are not commercially available and are currently in the early stages of materials development and prototyping. We were privileged to establish collaboration with Jens O. Jensen, of the Materials Science Group in the Department of Chemistry, of the Technical University of Denmark. This group provided us with a prototype high-temperature PEM fuel cell for testing with and integrated bed design and to demonstrate the operation with alanates. Details of the high-temperature PEM and the demonstration tests are presented in the following sections.

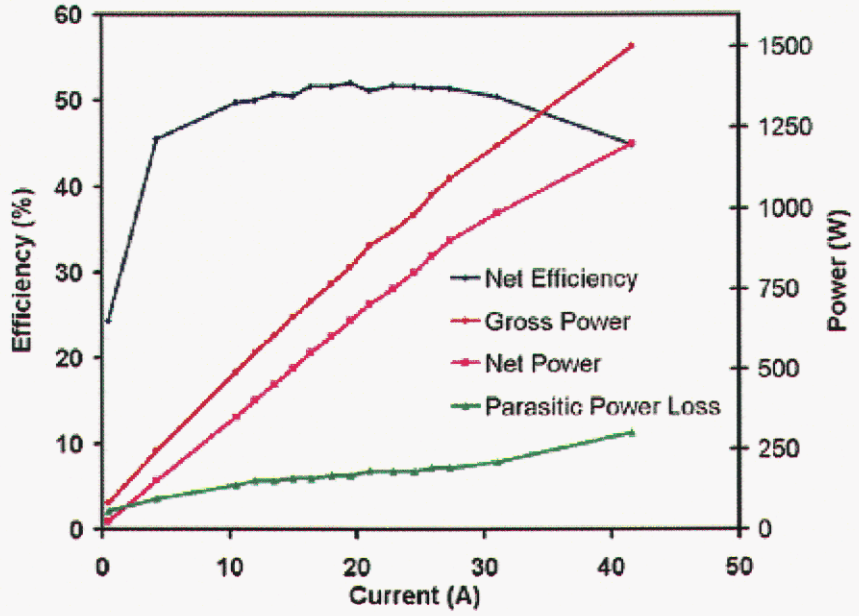

Figure 10. Nexa fuel cell performance and efficiency

2.2 Hydrogen storage material selection and properties

Sodium alanates are attractive due to their high gravimetric energy densities and was used as the dominant energy storage material in this demonstration. However, sodium alanates exhibit poor kinetics at room temperature. To use alanates to fuel either a low or a high-temperature PEM stack, the storage system will require a combination of materials (including complex and interstitial hydrides) to deliver hydrogen readily at temperatures below the optimum operation conditions. We used the stack warm up data obtained from the Nexa™ fuel cell system testing above to select an appropriate low-temperature interstitial hydride for cold-start applications.

There are a wide variety of interstitial hydrides that experience hydrogen sorption at appropriate temperatures for our application. Use of these materials for startup operation only overcomes the disadvantage of their low hydrogen capacities (1-2 wt.%) with respect to the alanates (4-5 wt.%). After reviewing the thermodynamic properties of common hydrides, it was determined that both TiFe and $MmNi_5$ (Misch metal – nickel) alloys fit the required target operating conditions (blue box in Figure 11). TiFe exhibits two plateaus, a lower plateau (alpha-beta) from 0.1-0.5 H/M and an upper plateau (beta-gamma) from about 0.55 -0.85 H/M. The lower plateau is very stable with cycling, but the upper plateau increases in pressure [29]. In addition, TiFe does not readily activate at room temperature. Heating to 400-450C under vacuum and 7 atm H_2 is recommended and several subsequent room temperature cycles may be required to reach full capacity [30].

On the other hand, Misch metal hydride ($MmNi_5$) exhibits a single plateau from about 0.1 to 1.0 H/M [31] and is very stable with cycling. The Misch metal - nickel alloy contains La:19.25, Ce:0.15, Nd:9.84, Pr:3.05, and Ni:68.07 in wt%. This alloy forms the basis for the active materials commonly used in nickel-metal hydride batteries and therefore is available from a variety of sources at relatively low cost. For these reasons, $MmNi_5$ was chosen for the cold-startup material. Santoku Metal America graciously provided 1kg of $MmNi_5H_6$ hydride for this research project.

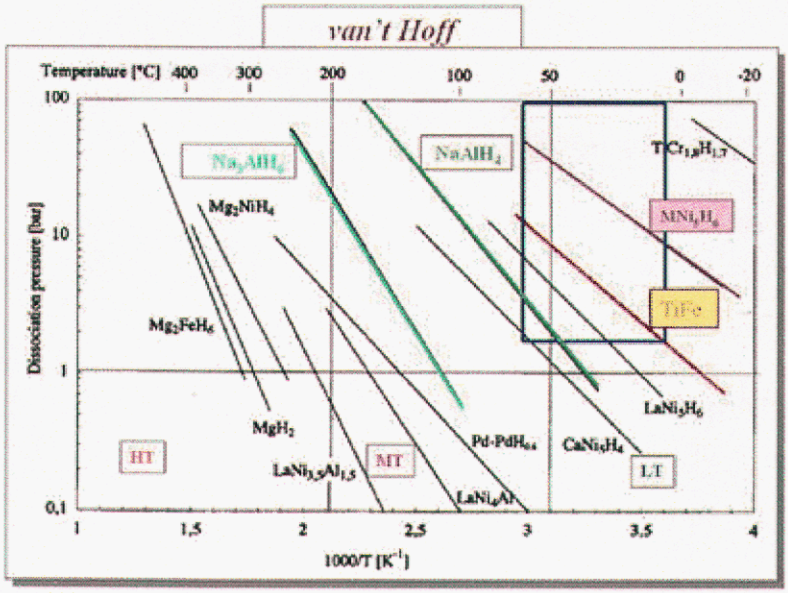

Figure 11. Plot of the equilibrium thermodynamic of a wide range of metal hydrides and the alanates. The blue box is the operating range as determined from the measured warm-up conditions of the fuel cell. Both TiFeH2 and MmNi5H6 fit the required thermodyamic properites, however MmNi5H6 is more practical in application.

2.2.1 Thermodynamic properties of selected materials

The thermodynamics of sodium alanate are well understood and described in literature [12]. An example of equilibrium PCT measurements of the alanates are given in Figure 5 for absorption and desorption. The enthalpy (ΔH) for the tetrahydride and hexahydride phases are 37kJ/mol and 47kJ/mol respectively [27,28].

PCT (Pressure Composition Temperature) isotherm measurements of the Misch metal-alloy were measured at various temperatures, ranging from 25 to 100 °C (results are shown in Figure 12). These measurements were done using a fully automated volumetric PCT instrument (PCTPro-1000, Hy-Energy, CA). One may note the appearance of a double plateau in the measurement, particularly at elevated temperatures. One possibility for this behavior is that the material

contains an inhomogeneous mixture of two phases with different compositions. However, a double plateau behavior is also commonly observed in this type of hydride due to the creation of crystal structure defects during the process of hydride formation. This latter effect is highly dependent on the hydrogen absorption and desorption conditions and may vary with measurement. The fact that the double plateau is not observed in the absorption at 81°C is a strong indication that the material is single-phase and that the double-plateau is due to defect formation.

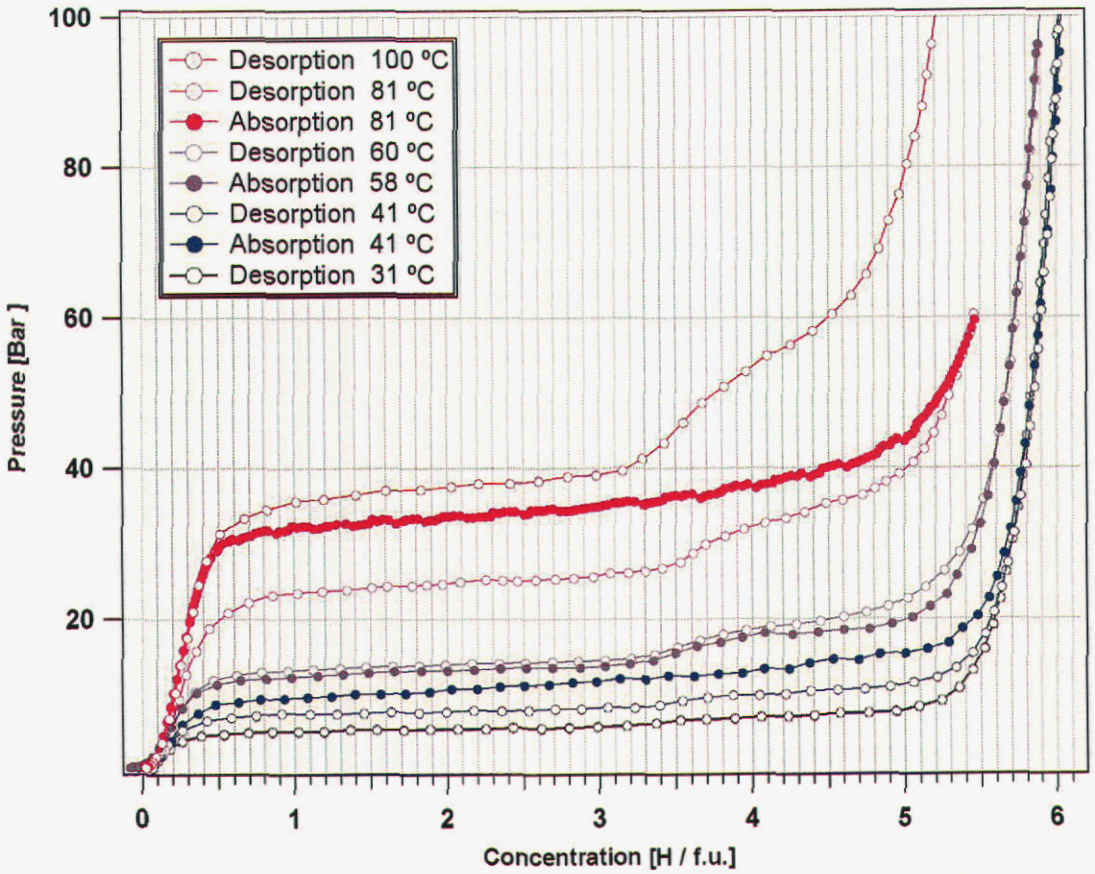

Figure 12. PCT measurements of MmNi5H6 determine that this hydride is appropriate for PEM fuel cell integration.

A van't Hoff plot (Figure 13, ln(Peq) vs. 1000/T) was generated from the above series of PCT measurements. The enthalpy of formation was derived from the slope of this equilibrium data. In this case, MmNi5 is somewhat less stable than LaNi5 (30 vs. 33 kJ/mol H2) and even less stable than $NaAlH_4$ (37k J/mol H2). This is desirable to allow for desorption at lower temperatures.

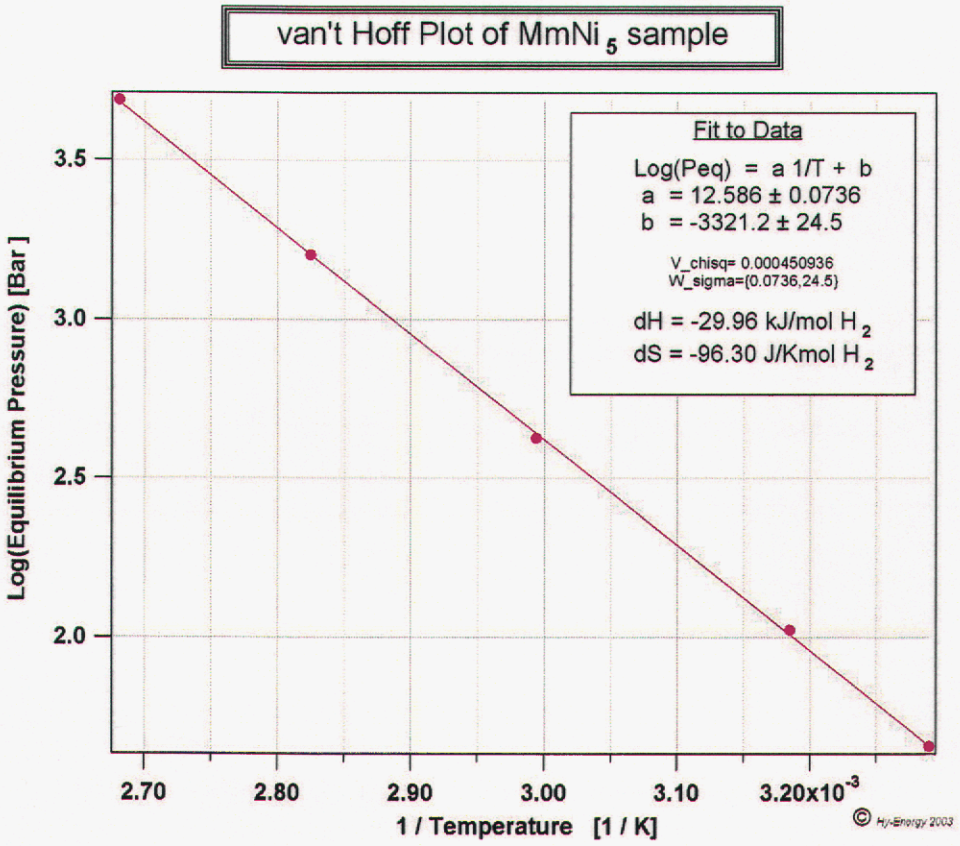

Figure 13. van't Hoff plot of the thermodynamics of MmNi5H6 hydride formation derived from the desorption PCT measurments.

The Mm-alloy works in combination with the alanate in the composite-hydride bed to provide hydrogen over a wide range of operational temperatures. The Mm-alloy generates between 2 and 10 bars in the typical range of ambient temperatures while the alanates will deliver a higher-capacity of hydrogen at the elevated operating temperatures of the fuel cell. Thus, the combined materials will provide hydrogen over the entire operational temperature range of the fuel cell stack.

2.2.2 Thermal properties of selected materials

The thermal conductivity properties of sodium alanates have been characterized using established techniques [32]. Properties for material compacted to 0.6 to 0.7 g/cc were used for thermal modeling of the bed.

The thermal conductivity of the Misch metal hydride was measured to support thermal modeling. The thermal probe method was used [32]. This method is well suited for low conductivity materials due to the transient nature of the measurement. This method does not require establishing or maintaining large temperature gradients, thus reducing the measurement time. The thermal conductivity was measured as a function of cycle as shown in Table 1.

Although the packed bed undergoes significant reductions in particle size during cycling, large changes in conductivity were not observed (measured at 4.5g/cc). After the bed was fully cycled and activated, the thermal conductivity was characterized as a function of gas pressure within the chamber. Results are shown in Figure 14 . Hydrogen gas pressures above 10 atm were used to avoid the endothermic release of hydrogen. To describe the thermal conductivity at lower pressures, helium was used for the bed in a fully desorbed state. The ratio between the two gas conditions can be assumed constant over the entire range [32]. The thermal conductivity varied nearly 100% over the entire measured pressure range due to the Knudsen effect [33]. The specific heat of the Misch metal was calculated from published values and estimated at 364 kJ/kg-K. Each elemental contribution to the specific heat was weighted according to the mass percent of that phase component for each relevant state (Table 2).

Table 1. Measurement of Misch metal hydride for 5 cycles demonstrates no significant change in thermal conductivity

Cycle	Kth (W/m-K)
1	1.49
2	1.45
3	1.56
4	1.34
5	1.55

Table 2. Heat capacity weighted mixture calculation of Misch metal hydride

Component	Wt%	Cp (kJ/kg-K) 83rd CRC
La	19.25	195
Ce	0.15	192
Pr	3.05	193
Nd	9.48	190
Ni	68.07	444
Weighted Mixture	100	364

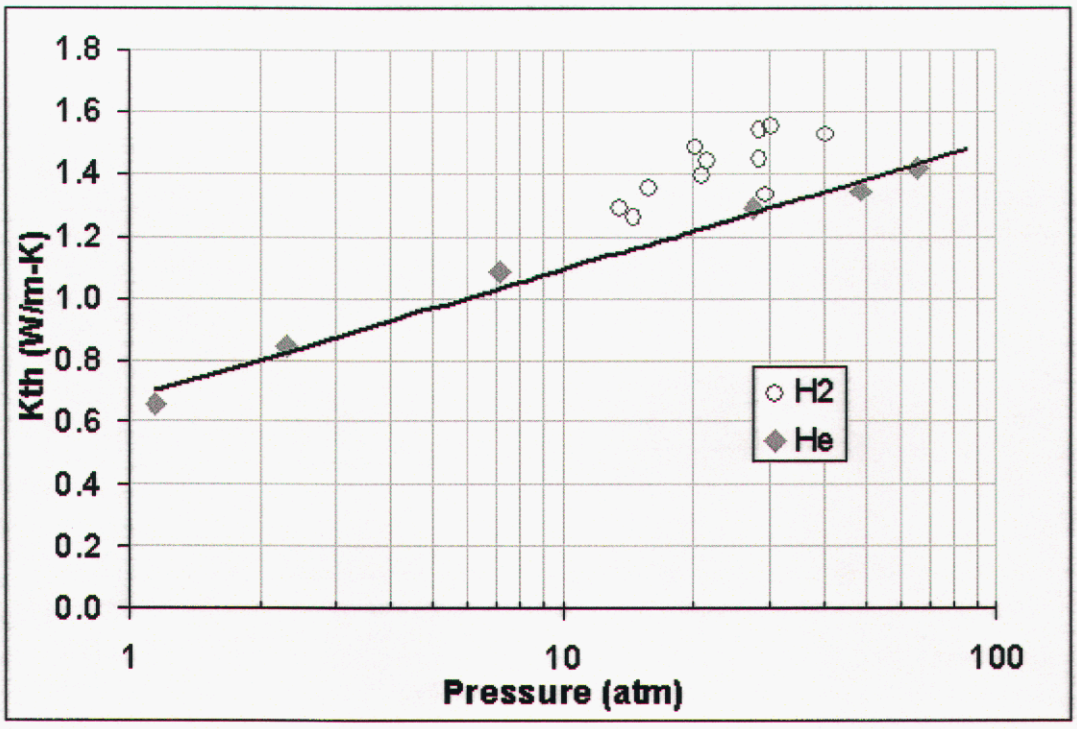

Figure 14. Thermal conductivity of Misch Metal as a function of gas pressure

2.2.3 Volumetric expansion of sodium alanate

Unconstrained Sodium alanates volumetrically expand during absorption by as much as 50%. The expansion can be limited by the vessel wall, however, the additional stress must be accomodated. Measurements have been made and reported for exerted pressures at various densities up to 1.0g/cc for capacities up to 2.3 wt% [34]. The highest pressures measured at this density totaled less that 6.9 bar (100 psia). This pressure is in addition to the gas pressure present within the system. These results also led us to a design parameter of 0.9 g/cc for the packing density of alanates in the final test beds.

2.3 Single-chamber bed design and fabrication

Single-chamber bed tests were designed to select the appropriate combination of alanates and Misch metal hydrides based on their thermodynamic and kinetic behavior.

A hydrogen storage bed was designed to meet the goal of direct heat transfer from fuel cell; flat surfaces on the outside of the bed were necessary for direct integration with a fuel cell stack. This first test bed includes a single chamber for hydrogen storage. The bed design was optimized for ease of loading and thermocouples were integrated to facilitate thermal data acquisition. The thermocouples were placed at various locations along the axial and radial directions to provide us with a description of the temperature field within the bed

during testing. Aluminum 6061-T6 was selected for fabrication of the single-chamber bed because of its superior thermal conductivity. As long as the alanates contain stoichiometric or greater aluminum content, then aluminum storage beds are appropriate for containing sodium alanate [35]. A cross sectional drawing of the single-cell bed can be found in the Appendix, Figure 36. Three dimensional finite element models were developed to calculate stress as well as thermal flow under operating conditions, as shown in Figure 15.

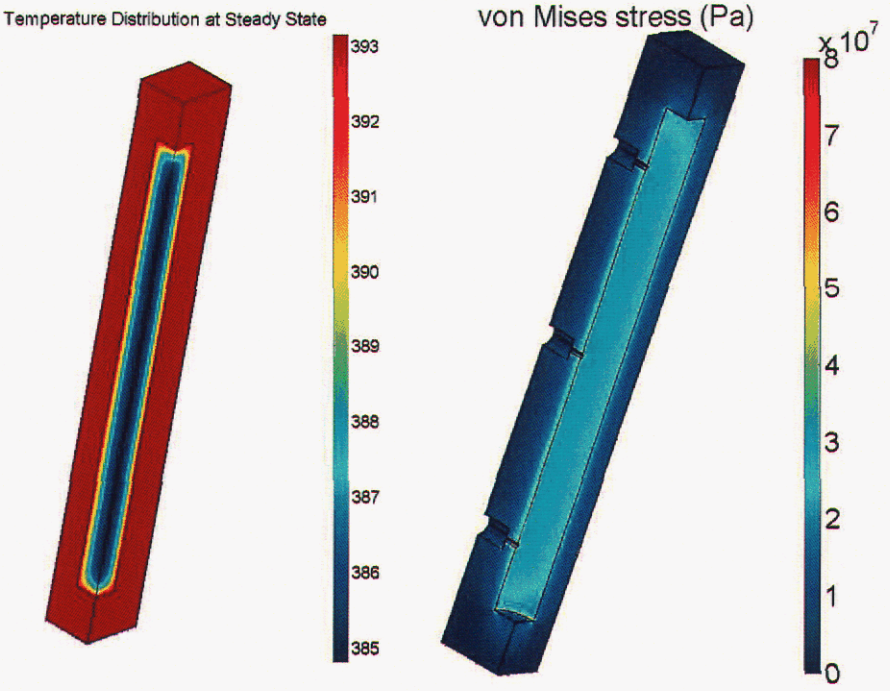

Figure 15. Finite element models of the single-chamber bed

Four test beds were built, each with a storage volume of approximately 30 cc. The single-cell bed is designed to 102 bar (1500 psia) with a safety factor of 4. The beds were leak checked at temperature of 150 C and proof tested to 1.5 times of the design pressure, 153 bar (2250 psia).

The single-chamber beds were modeled using the known and measured thermal properties of sodium alanate and $MmNi_5H_6$. Based on the characterization of the Ballard Nexa™ fuel cell, the amount of the exhaust heat available is calculated to be 0.363 W/cm^2. A tape heater with the capacity to produce up to 1.55 W/cm^2 was used to simulate the fuel cell exhaust heat and installed on the bed. The loaded beds were tested for hydrogen delivery performance and thermal flow. The beds were insulated with low density TEPIC structural foam (Sandia) machined to fit to the contours of the instrumented bed, as shown in Figure 17. The thermal conductivity of the foam (0.031 W/m-K) was measured using the thermal probe method [32,36] for accurate representation in the thermal model.

In preparation for the integrated system design, this experimental data was used to predict heating demands required to supply hydrogen in an integrated system, and the correct apportionment of interstitial hydrides and alanates.

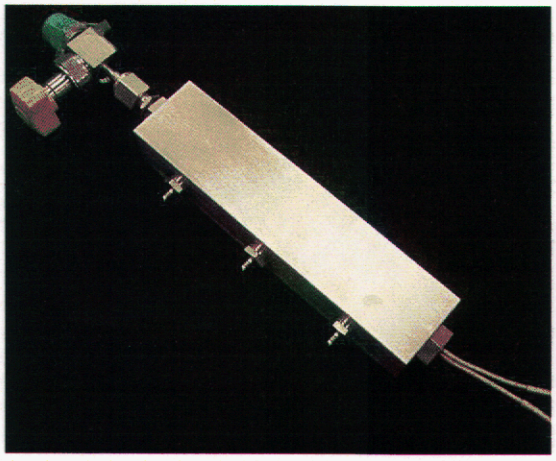

Figure 16. Finished single-chamber bed

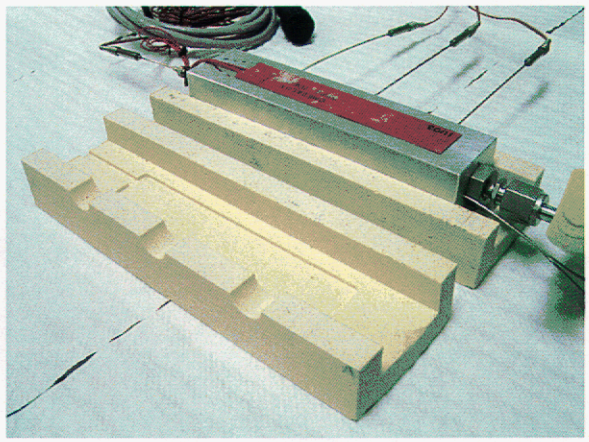

Figure 17. Bed insulated with machinable high-temperature foam

2.3.1 Single-chamber bed test results

Two single-chamber beds were loaded with $TiCl_3$-doped NaH+Al and $MmNi_5H_6$ respectively. Each bed underwent at least 10 sorption cycles in which capacity, kinetics, simulated heat input, and hydrogen delivery rate were measured.

2.3.1.1 Alanate single-chamber bed

The alanate single-chamber bed was loaded with 26 grams of $TiCl_3$-doped sodium hydride (NaH) and aluminum to form alanates through the direct synthesis method [20]. The average absorption and desorption capacity of this bed is 2.73 wt%. It took 24 hours or more to fully absorb hydrogen from fully desorbed state. We later learned that that a large initial aluminum particle size (149μm) and insufficient mechanical milling time (<4 hours) caused the lower-than-expected capacity in this material.

Based on 26 grams of sodium alanate and 2.73 wt%, the amount of hydrogen stored in this bed is 0.71 grams. From the characterization of the commercial fuel cell as described in section 2.1, this bed should be able to supply 10 W fuel cell for approximately 1 hr at 0.132slpm. To ensure test results applicable for actual fuel cell operation, desorption pressures ranged from 1 to 2 bars of initial pressure. This will meet the requirements for fuel cell operation.

A range of added heat flux and desorption temperatures were tested. All tests were performed starting from room temperature. The average hydrogen delivery rate in the first hour of desorption vs. heat input is plotted in Figure 18. Our fuel cell characterization indicated that 50% of the fuel cell power is available as exhaust heat, or 10.8 W. The measured flow rates demonstrate that the kinetics of this material are too slow to allow for hydrogen delivery from room temperature. Thus, a combination of materials is required for startup. Large gains are also realized from operating at a higher temperature as shown in Figure 18.

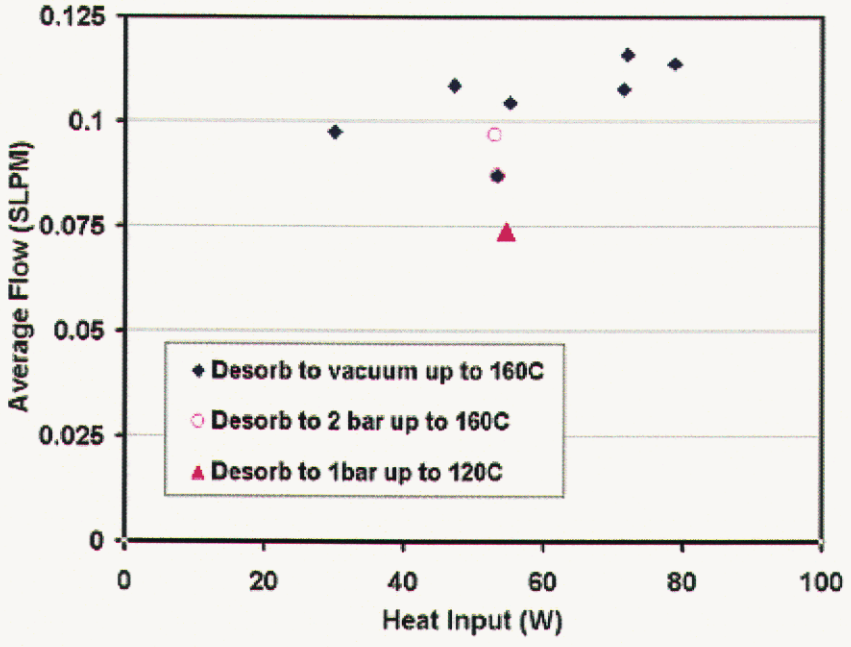

Figure 18. Single-chamber sodium alanate bed hydrogen delivery rate vs. heat input

2.3.1.2 Misch metal single-chamber bed

The Misch metal single-chamber bed was loaded with 163 grams of $MmNi_5H_6$. The average absorption and desorption capacity of this bed was 1.23 wt%, and it took approximately 4 hours to fully absorb hydrogen from the fully discharged state. This was due to the limited heat transfer out of this simple bed design.

Based on 163 grams of $MmNi_5H_6$ and 1.23 wt%, the amount of hydrogen that can be stored in this bed is 2.0 grams. From the characterization of the commercial fuel cell as described in section 2.1, this bed should be able to supply 167 W fuel cell for approximately 10 minutes at 2.225 slpm. Similar to the alanate tests above, desorption pressures ranged from 1 to 2 bars, as required in most fuel cell operation. All tests were performed starting from room temperature. Different levels of heat input and desorption temperatures were tested. The average hydrogen delivery rate in the first hour of desorption vs. heat input is plotted in Figure 19. From these measurements, based on available fuel cell heat of 166.5 W, it was determined that the kinetics of this material will work well with any PEM fuel cell, as well as for cold-startup in combination with the alanates.

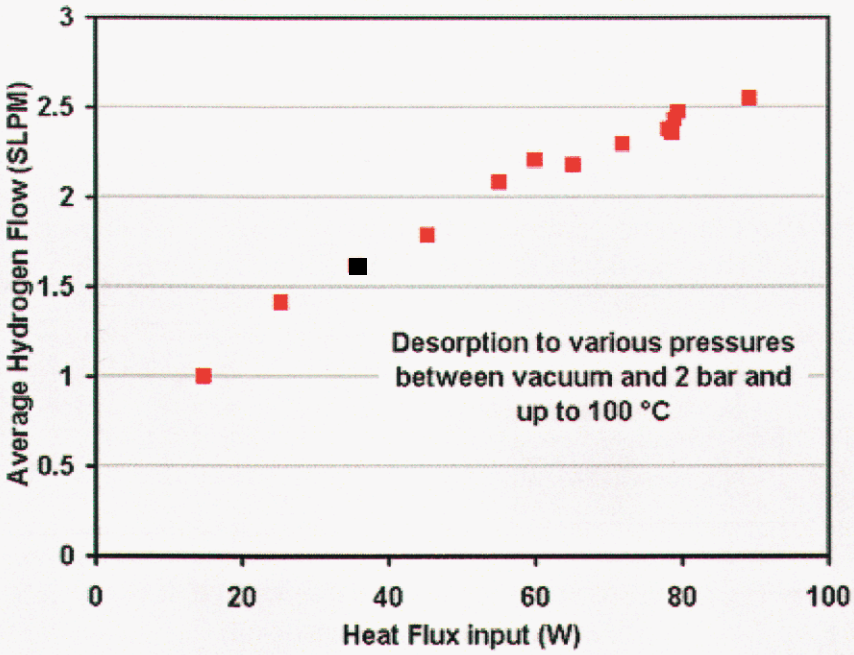

Figure 19. Single-cell MmNi5H6 bed hydrogen delivery rate vs. heat input

Data from these two test beds were combined with the experimental materials characterization above to produce the parametric information required for the modeling to design and develop a fully integrated system.

3 High temperature fuel cell characterization

A prototype high-temperature fuel cell stack was acquired from the Technical University of Denmark. The operating temperature of this stack (150 to 200 °C) is well suited for integration with a sodium alanate storage bed. Sodium alanate requires at least 160 °C to attain useful kinetics and this prototype fuel cell requires similar temperature for optimum efficiency. The stack was characterized in Denmark and repeated upon arrival at Sandia National Laboratories, California. A description of the stack and the results of this characterization are presented below.

3.1 PBI: Higher temperature membrane material

Conventional polymer fuel cells utilize a polymer electrolyte membrane, which is made of a perfluorosulfonic acid (PFSA, e.g. Nafion™). The conductivity of PFSA relies on gas humidity and is restricted to operating temperatures below 100 °C (80 °C operating temperatures with reactant gas humidification is typical).

Unfortunately, these operating temperatures are not ideal; higher temperatures allow for higher efficiencies, greater CO tolerance [38], and for this application, sufficient quality of heat for hydrogen evolution from the storage beds. To overcome the temperature limitations of typical membranes, a novel organic polymer structure must be used. The most successful option to date is polybenzimidazole (PBI) doped with phosphoric acid (repeating structure shown in Figure 20). Development of PBI based fuel cells at the Technical University of Denmark have resulted in the demonstration of system with operating temperatures up to 200 °C [39]. A general review on high temperature polymers has also been compiled by Li et al [40].

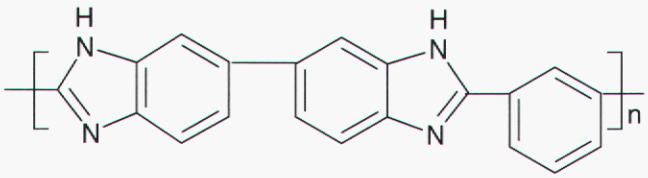

Figure 20. The repeating unit of the high temperature PBI, poly 2,2´-m-(phenylene)-5,5´-bibenz-imidazole.

3.2 Stack Assembly

A six cell stack was assembled by the Technical University of Denmark for this demonstration. The anode and cathode electrodes were catalyzed with an approximate platinum loading of 0.5 mg/cm^2. The 50 µm membranes were clamped between 2cm thick aluminum endplates complete with cooling channels. A thermocouple was placed in the center of the stack between cell 3 and cell 4 where the highest temperatures are experienced.

3.3 Initial stack validation tests

The stack was tested at the Technical University of Denmark while supplied with hydrogen and pure O_2 and as well as hydrogen and air. The unheated gasses (research grade) were introduced using electronic flow controllers and were allowed to flow open-ended through the stack. No humidification of the gasses is necessary when PBI-based membranes are utilized.

The stack was heated with resistive heaters and maintained at approximately 150 °C. Polarization curves from this testing is shown in Figure 21 and Figure 22. Using air and hydrogen as reactant gasses, 50 W of usable power is easily produced.

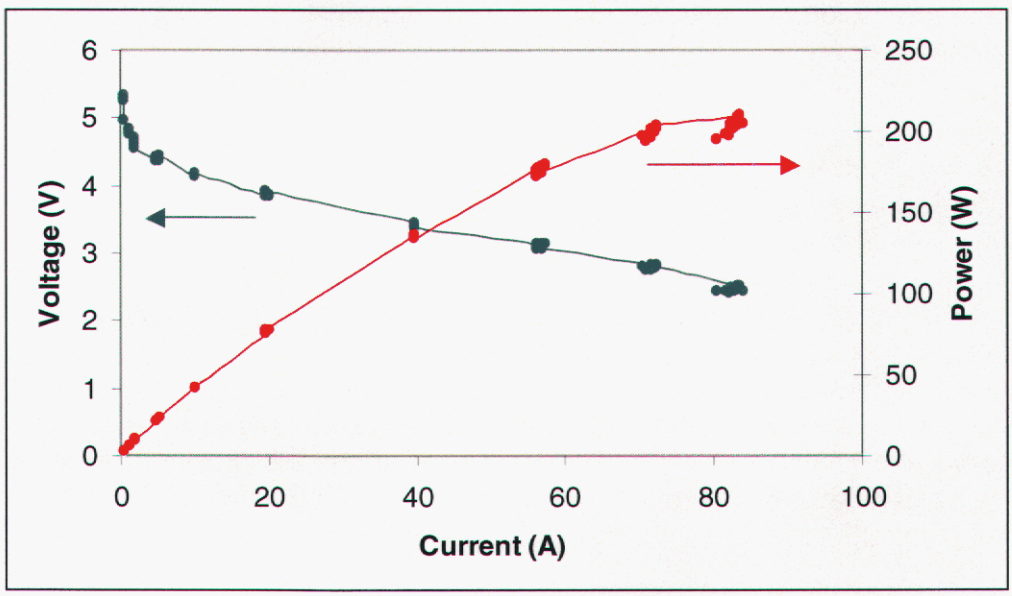

Figure 21. Voltage and power of the 6 cell stack operated on H2 and O2 (8.3/8.3 SLPM) at about 150 °C.

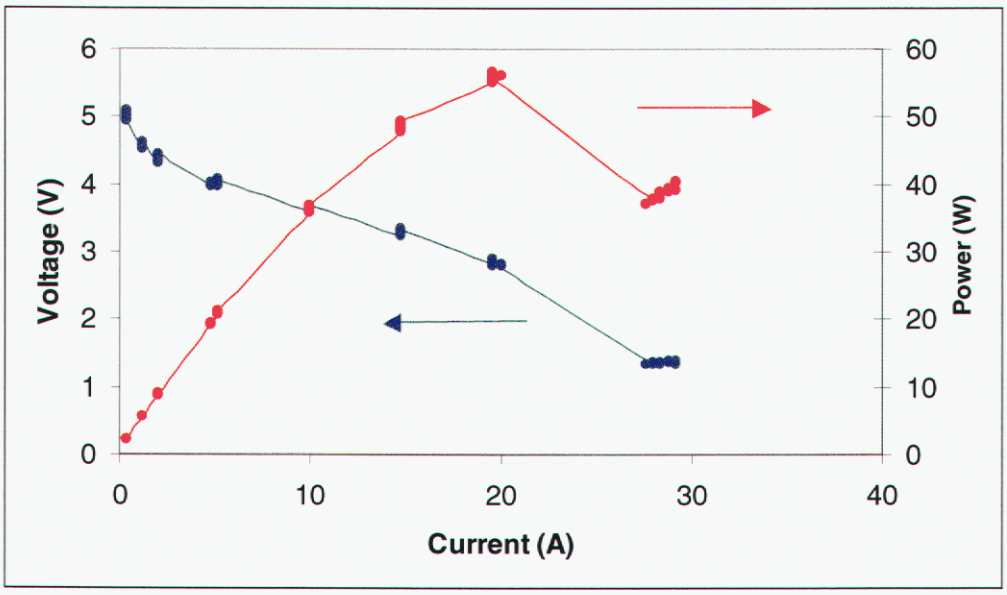

Figure 22. Voltage and power of the 6 cell stack operated on H2 and air (8.3/11.6 SLPM) at about 150 °C.

3.4 PBI fuel cell testing at Sandia National Laboratories

A custom manifold was built for the operation of the high temperature fuel cell integrated system demonstration. Reactant gases were sourced from high-purity, high pressure tanks to insure that the stack would not be compromised from the exposure to contaminated gasses. Both the air and hydrogen manifolds contained mass flow controllers and meters calibrated to their respective gases (see the Appendix, Figure 37). Additionally, the input gas pressure was monitored with calibrated 0-50psi transducers and pressure relief valves were installed to protect the stack from pressures exceeding 3-4psi over atmosphere. The manifold was designed to accommodate the storage beds that would be integrated into the system later in the project (this is shown in Figure 37). A Dynaload™ adjustable resistor bank (Transistor Devices, Inc.) was used to provide a load for the fuel cell. The instrument was operated in constant current mode (current held constant regardless of voltage) during the characterization of the fuel cell to generate the power-voltage-current curves.

When fuel cells are run in the dead-end mode, it is necessary to occasionally purge the hydrogen line to clear any vapor and condensed water that has gathered within the flow lines. This process was automated using an electrically actuated pneumatic valve and power supply controlled through a Labview™ code written for this application. During normal operation, the fuel cell benefited from a 1 second purge on a frequency of 30 to 120 seconds depending on the reactant consumption (power output) of the fuel cell. Fuel cell voltages, current, temperature, flow rates, and reactant gas pressures were measured and recorded with a Agilent multimeter (model #34970A) and data acquisition

package (Benchlink™ Datalogger). The fuel cell current was measured with a calibrated resistor with a response of 50mV per 50A.

We recreated the performance curves provided by the Technical University of Denmark in an effort to validate our custom manifold. Our tests results demonstrated equivalent performance with a peak power of approximately 55W at 8.8 LMP H2 and 8.3 LMP air (open ended). Since open flow is not a valid scheme for our application, we also investigated the optimum flow conditions for closed-end hydrogen flow. The peak power optimum closed-end flow rates were found to be 0.8 and 5 LMP for hydrogen and air flow respectively. The optimum operating temperature was found to be 160 °C although higher temperature may have resulted in improved performance but reduced membrane life. These conditions resulted in a peak available electrical power of approximately 37W and are appropriate for demonstration in conjunction with the hydrogen storage beds. Power-voltage-current curves for these operating conditions are shown in Figure 23 for both open and closed end operation.

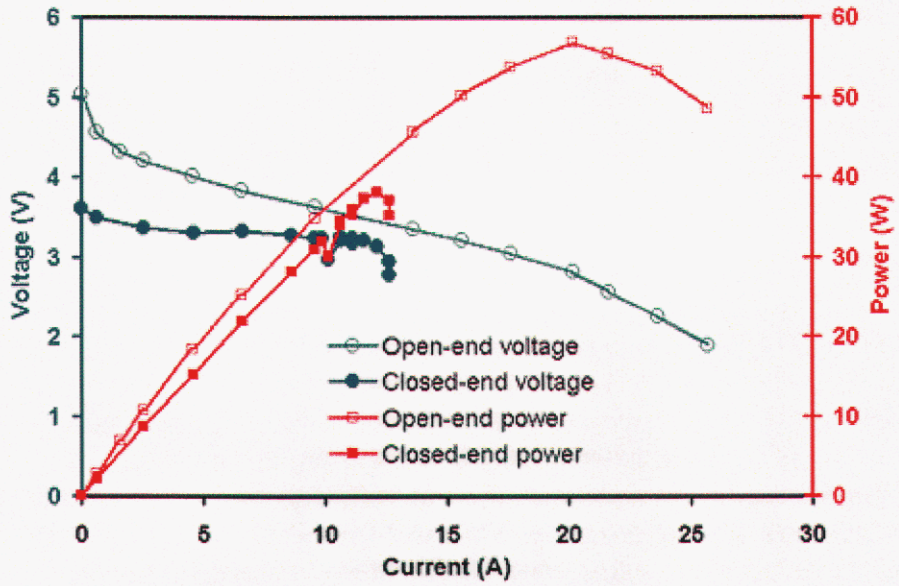

Figure 23. Voltage-Current-Power curves comarison for open-ended and closed-ended operation at 160 °C. Open ended H2/Air flow = 8.8/8.3 SLPM. Closed ended H2/Air flow = 0.8/5.0 SLMP.

4 Integrated bed design and operation

The reader is reminded that the main goal of this project was to demonstrate a small stand-alone power pack that can be quickly charged with hydrogen from a standard gas bottle. Toward this end, a storage bed was designed and optimized to accommodate the high temperature fuel cell from the Technical University of Denmark. The learning gained from the single-chamber bed testing was used in the design to specify the required characteristics of a fully integrated bed to supply the fuel cell with hydrogen.

4.1 Design requirements of the integrated storage bed

Solid-state hydrogen storage materials and fuel cells energetically compliment one another. The fuel cell requires heat removal, while the storage bed requires heat addition to maintain the evolution of hydrogen. Thus, when intimately integrated, the components of the system are energetically beneficial and the quantity of heat transfer hardware is reduced (heat exchanger, heat transfer fluid, etc. is not required)

The acquired stack is shown in Figure 24 as received from the Technical University of Denmark. This stack was particularly useful for our integration efforts due to the higher operating temperature (up to 200 °C) which is appropriate for sodium alanate hydride decomposition. The stack came fully assembled between two 2cm aluminum plates that were bolted together to seal the stack. Sandia National Labs agreed to not modify or disassemble the stack to protect the intellectual property associated with this prototypical stack. The storage beds were designed to accommodate the plates, bolts, and flow paths. This is not ideal, as the plates add considerable thermal load to the system (on order of 2200J/K). Future work should include collaboration with the stack developers to optimize the structural components of the system to minimize their effect on heat transfer. Theoretical optimizations of the stack and storage bed are described in the sections below.

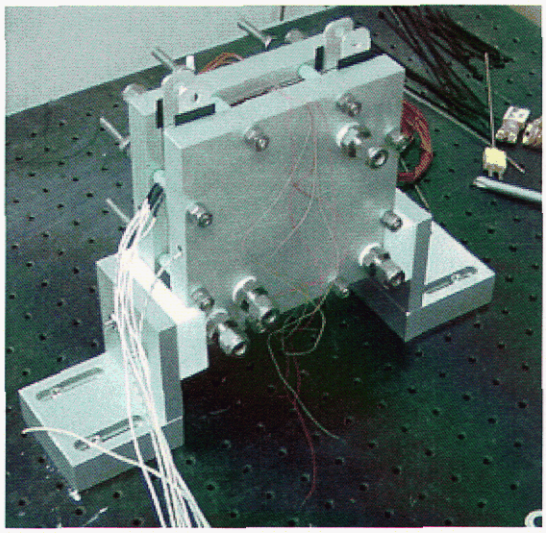

Figure 24. Fuel cell stack as recieved from Technical University of Denmark

The beds were designed to provide sufficient hydrogen flow to the stack for 40 to 60 minutes. As described in the stack characterization section, 0.7 to 0.8 LPM of hydrogen must be provided continuously to the stack requiring a total of up to 48 standard liters of available hydrogen.

4.2 Structural optimization of the storage bed

The storage bed was designed to provide up to 1.2 SLPM of hydrogen for 40 minutes. This required 173g of sodium alanate in both beds assuming a usable wt% of 2.5.

Stainless steel and aluminum have both been used extensively for sodium alanate hydrogen storage beds. Although more exotic materials may be appropriate, these two options are proven materials for this role and are straightforward to fabricate. They are compatible with these hydrogen storage materials, and have relatively high strength to weight ratios. Aluminum is compatible with sodium alanate as long as the alanate chemical composition is stoichiometric [35]. The bulk of the bed was fabricated from 6061-T6 aluminum to optimize the heat transfer between the fuel cell and the storage bed.

A commercially available finite element code (FEMLAB™ 3.0) was used to optimize the bed structure to withstand 413 bar of pressure, four times the maximum operating pressure, 103 bar. The most efficient chamber structure is the equilaterally close packed structure. This is easily shown by comparing the two structural models, one with a linear coordination, and one with an equilateral coordination. Figure 25 demonstrates that if the storage chambers are linearly coordinated, excessive stress (171 MPa) is experienced within the intermediate members at a gas pressure of 413 bar. This stress is not highly sensitive to the external wall thickness and the internal members are in tension (weaker compared to compression). However, when the chambers are coordinated equilaterally, the stress is distributed effectively as the internal members are subject to compressive forces and less structural bulk is required. The final design shown in Figure 26 shows a maximum stress of 102 MPa at a gas pressure of 413 bar, which meets the tensile strength requirements of 6061 series aluminum at 200 °C (103.5 Mpa) [36].

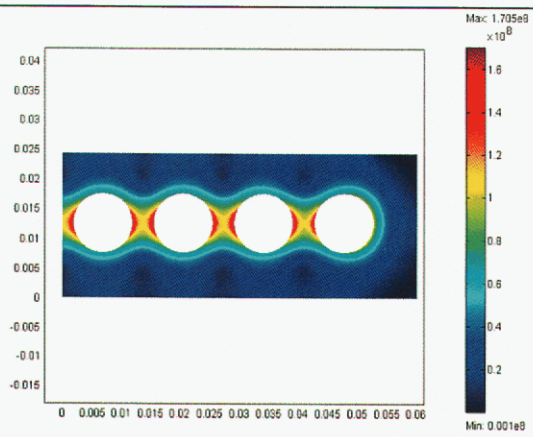

Figure 25. Linear coordination of storage chambers leads to excessive stress in intermediate structural members

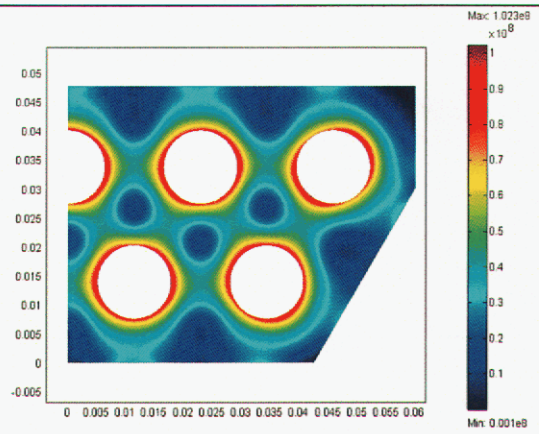

Figure 26. Equilateral coordination of the storage chambers effectively distributes stress

The cap to the chamber was also modeled and optimized to a thickness of 2cm. It is helpful to note that the bolt preload should always be designed to exceed the pressure load, thus keeping the bolt from elongating and acting as a spring. This can be easily modeled by constraining the bolt head area in the axial direction of the bolt. The solid model of the final design is shown in Figure 27. The system was pressure tested to 1.5 times the maximum allowable working pressure (155 bar).

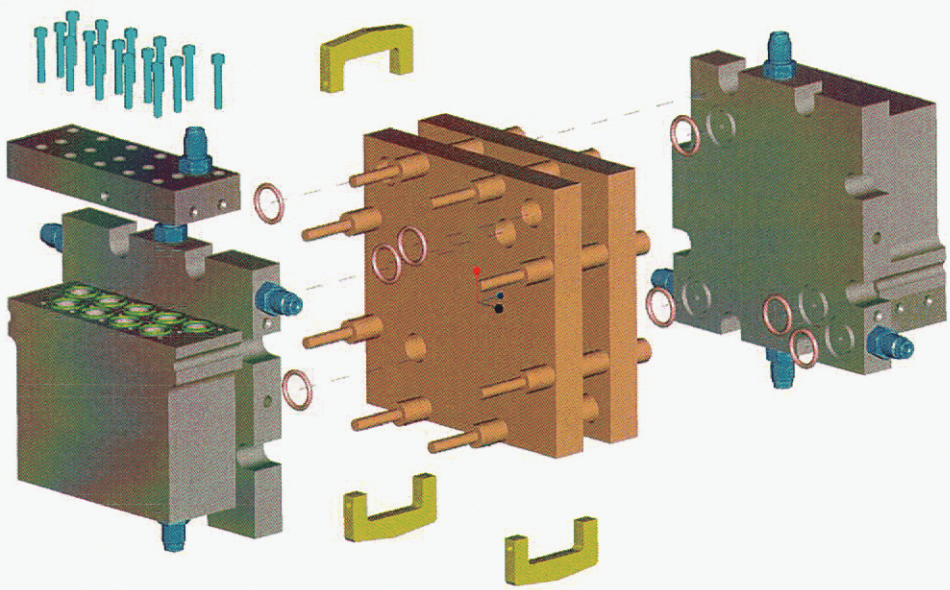

Figure 27. Solid model of final storage bed and fuel cell integration

4.3 Thermal modeling of the structurally optimized bed

Prior to testing and fabrication, a three-dimensional thermal model (Figure 28) was constructed to predict the performance of the system when operated with the fuel cell. The thermal model included system insulation (not shown in Figure 28) and assumed perfect contact between the fuel cell plates and the storage bed. The gas flow paths, bolts, and fuel cell stack features were not modeled to avoid unnecessary computational complexity. The model was used to predict the performance of the optimized bed after integration with the high temperature fuel cell.

4.3.1 Theoretical steady-state performance for the integrated bed

A steady-state predictive model was assembled to determine the largest temperature drop in the bed due to the endothermic reaction of the sodium alanate during fuel cell operation. Perfect contact was assumed between the fuel cell and the storage bed and between the storage bed and the low density TEPIC insulation. The outer surface of the foam was assumed to have a heat transfer coefficient of 5 W/m^2-K. The initial temperature of the aluminum bed was assumed to be 433K. To determine the heat required to sustain the reaction for a constant flow rate of 0.8LMP, the heat of reaction was assumed to be a constant 37 KJ/mol. This equates to a volumetric heat sink of 107 kW/m^3.

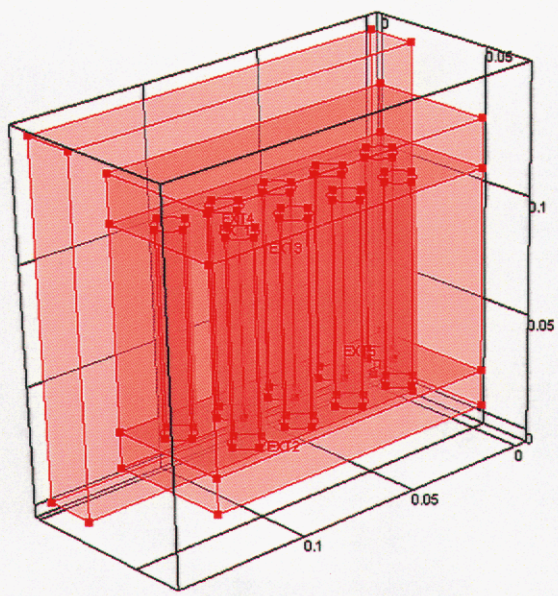

Figure 28. Thermal model of storage bed including sodium alanate and Misch metal hydride (insulation included in calculations but not included in the image)

Assuming a constant usable fuel cell power output of 35W and a waste heat output of 50W, the heat input to each bed is 1113 W/m^2 at the fuel cell boundary. Under these conditions, modeling demonstrates that the system is self-sustaining, not requiring auxiliary heat input. The highest temperature drop seen in the system is 4 °C at approximately 200s during a 1 hr operation simulation. This small temperature drop would not have a significant effect on hydrogen flow.

4.3.2 Theoretical startup performance for the integrated bed

Simple calculations were made to determine the feasibility of cold startup for this system. The heat load of each major component of the system was calculated to determine the time required to heat the system to operating temperatures. Perfect insulation was assumed and the polymer cells were neglected. For these calculations, 2 of the 18 chambers are filled with Misch metal, while the rest contain sodium alanate. Figure 29 describes the energy required to heat each component by 60 °C. These calculations do not include the energy requirements of support the endothermic reaction. The aluminum bed and the end plates dominate the amount of energy required. A startup time of 2.5 hrs would be required to heat this system from 100 to 160 °C with 50W being supplied from the fuel cells. This is clearly an unreasonable time and future work would reduce the heat load required to realize the startup capabilities of this system. See the following section for recommendations to reduce the heat load of this system by over 70%.

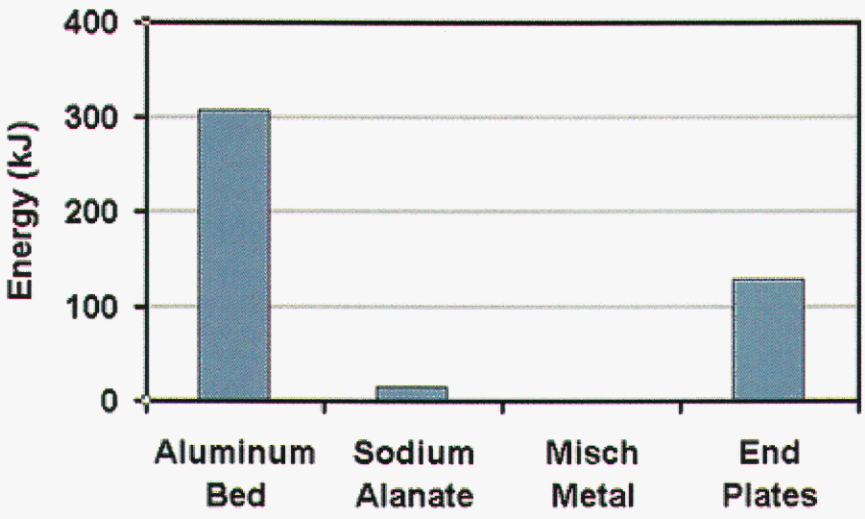

Figure 29. Comparison of energy required to raise temperature of system by 60 °C, neglecting the the polymer cells and assuming perfect insulation

As described above, cold start-up is not feasible using this non-optimized system as determined by simple heat capacity analysis. However, a transient model allowed us to determine if different fuel cell operating conditions and performance would allow us to utilize the waste heat for heating the system to operating temperature. For the first simulation, a 35W fuel cell operating at 41% efficiency (50W total heat, constant output) was assumed. The environment surface was assumed to have a heat transfer coefficient of 5 W/m^2-K. Also the fuel cell plates were neglected as these add considerable heat load and presumably could be avoided in future system designs. The startup conditions were simulated in a three step process shown below.

Conditions	Output
Stack and beds at 80 °C, environment at 20 °C	Initial conditions for Misch metal desorption
10 min supply from Misch metal chamber	Initial conditions for alanate steady state operation
Steady state operation	Final solution

For these conditions, the heat load of the system is quite significant and the waste fuel cell heat does not contribute a significant amount of the energy required. The system is only heated by about 3 °C in 10 minutes. To improve this scenario, two recommendations are made: 1) reduce the parasitic heat load of the system, and 2) use the heat from the fuel cell during startup as an assistance to a secondary auxiliary (Joule or catalytic) heating scheme.

4.4 Storage bed integration with high-temperature stack

The beds were loaded with 173g of alanate at ~0.9g/cc initial packing density. Material preparation properties and components are shown in Table 3

Table 3. Sodium alanate production parameters

Material preparation method	Direct synthesis planetary milling in tungsten carbide mill
Milling time	4 hrs in Argon environment at 250rpm
Composition	51.85 mol% NaH + 46.30 mol% Al + 1.85 mol% TiCl3
Aluminum particle size	20 μm
Packing density	0.9g/cc

Prior to integration, the full cycle capacity of the bed was characterized using a custom Sieverts apparatus in the Hydride Characterization Laboratory at Sandia National Laboratories. The fully cycled capacity was just over 3 wt% (material only, system weight not included). The integration of the system is shown in Figure 30 and Figure 31. The mating surface of the bed and stack was coated with thermal grease (Omega 201) to insure optimum thermal contact. The system was held together mechanically using fabricated "C" style clamps. All stand-alone flow functionality of the stack was retained (reactant and coolant gasses). Figure 31 shows the system when insulated using machinable TEPIC low density foam (in-house recipe, Kth = 0.07W/m-K).

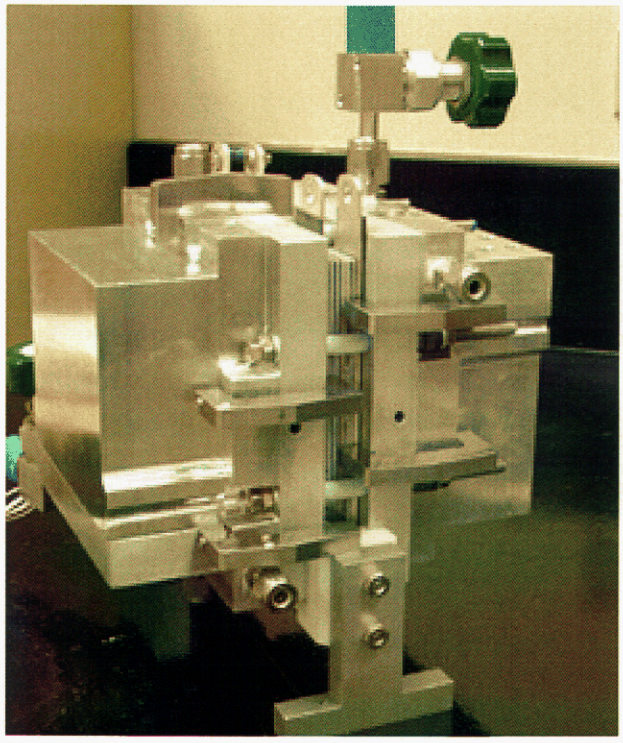

Figure 30. Integrated storage bed and stack, without plumbing

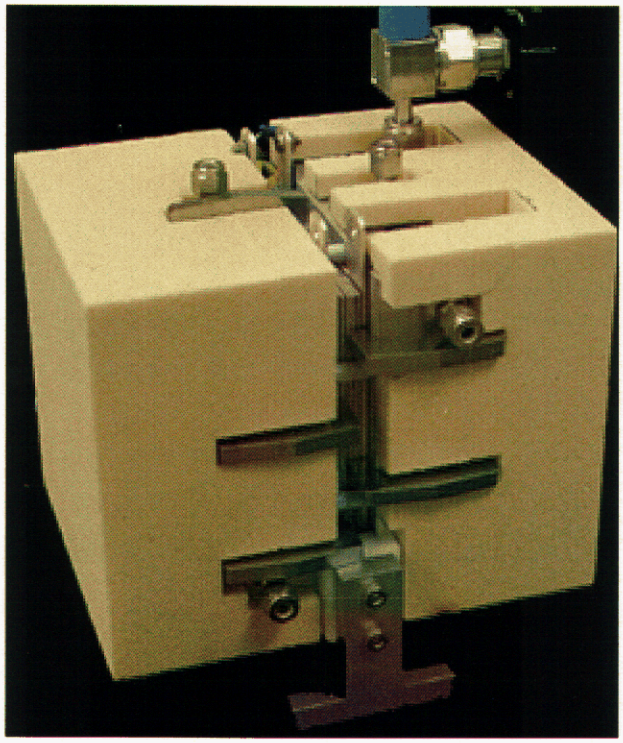

Figure 31. Insulated system (TEPIC low density machinable foam)

After integration, the stack did not perform nearly as well as observed during the stand alone tests. With aid from our colleagues at the Technical University of Denmark, it was determined that the membrane had suffered some damage. This was confirmed when excessive hydrogen and air mixture was observed in the exhaust lines. Despite this, the stack was still able to operate at a nominal flow levels, however, we were required to use open hydrogen flow (rather than dead-ended) without optimized purging found during the characterization tests. We did find it helpful to close the hydrogen valve for 1 second on an interval of 70 seconds.

4.5 Steady-state performance of the integrated system

A total of two tests were conducted with steady-state conditions. The system was heated to 160 °C using the hydrogen and air high pressure sources until equilibrium was reached. The hydrogen was then sourced from the storage beds and flow was controlled through the manifold mass flow controller. Test results are given in Table 4

Table 4. Integrated storage bed and fuel cell demostration

Test #	Absorption time (hrs)	Flow (SLPM)	Operation time (min)	Usable Hydrogen	Ave Power (W)
1	121	0.77	65.8	4.55g (2.6 wt%)	6.9
2	14	0.80	62.6	4.50g (2.6 wt%)	3.5

Observe that even though the absorption times of test 1 and 2 vary by an order of magnitude, the beds contain nearly identical quantities of usable hydrogen (2.6 wt%). This implies that during absorption, usable compounds of hydrogen form quickly, and during desorption, phase separation happens as a function of hydrogen evolved and not as a function of phase. Test number 2 resulted in the most consistent power output from the fuel cell, although the amount of power was considerably lower (3.5 W compared to 6.9 W in test 1). The performance of the system can be seen in Figure 32. During this test, hydrogen was detected in the air exhaust and air was also flowing out the hydrogen exhaust indicating an internal membrane failure. The periodic spike in the fuel cell power output was due to the purging cycle of the hydrogen line. Overall, the demonstration was overwhelmingly successful, showing that a fuel cell can be supplied with hydrogen from sodium alanate for up to 2.6 wt % of the material. Although this fuel cell was not operating at optimum power, enough hydrogen was evolved to fuel a 50% efficient fuel cell producing 71W of usable power for over one hour.

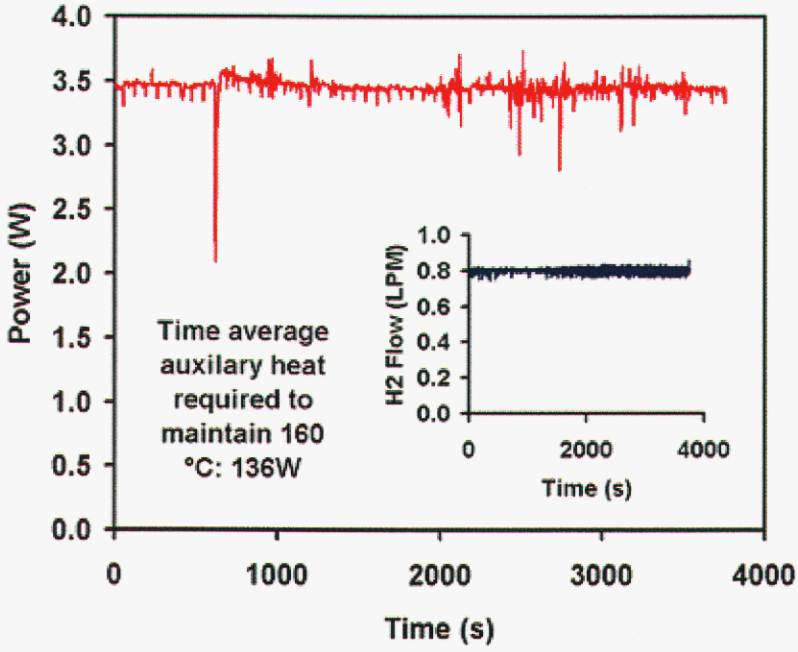

Figure 32. Integrated storage bed and stack performance

Auxiliary heat flux required to keep the stack at 160 °C was measured during the test. On average, 136W of heat was added to the system with a resistive heater. Since minimal heat was being contributed by the malfunctioning stack, the benefit of intimate integration is not immediately apparent. However, if we assume that the stack was 50% efficient and producing 71W of heat, this would reduce the energy requirements to evolve hydrogen by over half. Additionally, a fully parallel integration of a complete stack would reduce and the heat lost to the environment and simplify insulation, thus reducing or eliminating the auxiliary energy required to maintain the system at operating temperature.

4.6 Cold-start performance of the integrated system

A cold start scenario was simulated using the integrated bed. In this scheme, 2 chambers were filled with Misch metal (81.31g) and the remaining 16 were filled with sodium alanate (144.25g). Unfortunately, because the stack was damaged only a few watts of usable power (and thus heat) could be produced. In order to accommodate this during testing, resistive heaters were utilized to simulate the stack heating process (500W total). The system was first warmed to 100 °C and the stack was allowed to equilibrate using the manifold reactant gasses. Hydrogen was then drawn from the Misch metal beds while the system was heated to 160 °C using auxiliary heaters. The hydrogen was fully depleted from the Misch metal in 24 minutes (1450 seconds) and at this point, the hydrogen flow was taken from the alanate. During the entire test, hydrogen flow remained at a stable 0.8 SLMP which, according to our earlier characterization of the fuel cell, would provide 71 Watts of useable power.

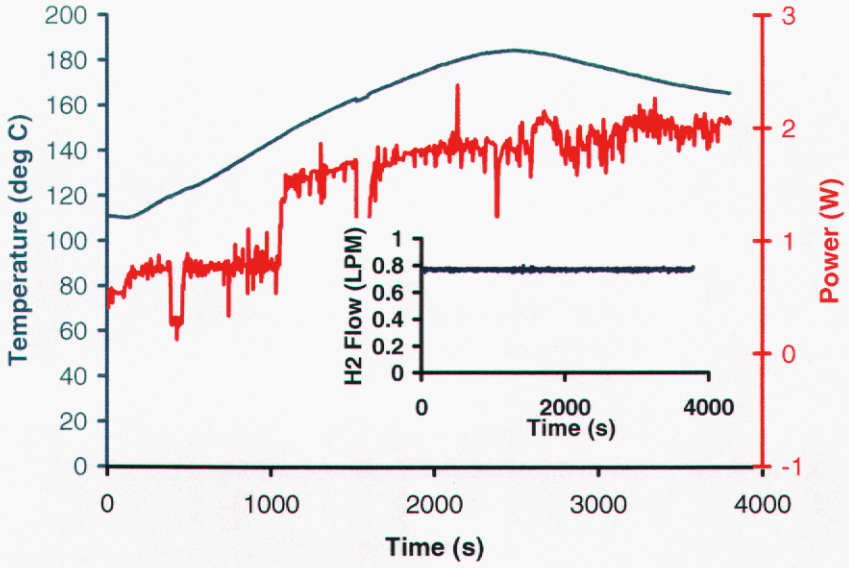

Although the measurements were performed with a damaged fuel cell, this test demonstrated that the scheme of combining hydrides with appropriately different thermodynamics, results in an energetically optimum arrangement for the continuous delivery of hydrogen from solid state sources at variable temperatures.

4.7 Recommendations and designs for future studies

This initial project goal was proof of concept. This was successfully achieved in large part through the use of the high-temperature PEM fuel cell. Future work to bring this technology to the point of world-wide recognition would focus on optimizing the system to demonstrate the potential for greatly enhanced performance over current fuel cell / storage system technologies. This work would be done in coordination with the high-temperature fuel cell developers to design and build an integrated and fully optimized system.

The following are the most important modification that would be addressed to significantly improve performance. First, the large aluminum plates that are currently used to clamp the stack together could be eliminated and combined with the functionality of the storage bed. This would reduce the heat load required for heating the system by 29%. Additionally, the storage bed should be made of stainless steel rather than aluminum. Although aluminum has a higher thermal conductivity and lower density, its relatively low strength at 200 °C (103.5MPa) requires excessive structural bulk. For comparison, a preliminary design of a stainless steel bed was developed. The structural components of the bed are made of 304 series stainless steel surrounded in a thin aluminum jacket for heat distribution. The 2.22cm OD stainless steel pipe has a wall thickness of 1.65mm and is 8.6cm long. The vessel MAWP is 2800psi. The tubes are welded into the flange plate as shown in the solid model of this design (Figure 33).

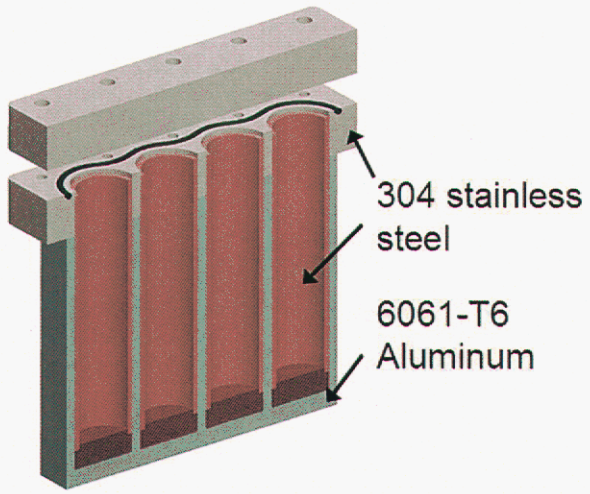

Figure 33. Proposed bed design uses stainless steel for structural members and aluminum to distribute heat

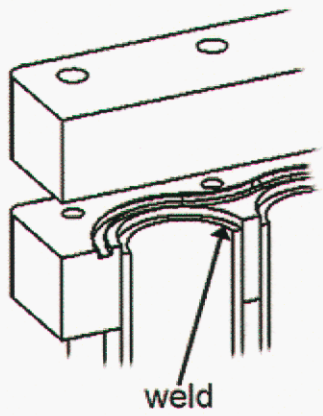

Figure 34. Weld detail for proposed stainless steel bed

The two beds can be compared based on their heat load on the system. The backing plates that mate with the stack plates shown in Figure 27 are neglected. The geometry of this plate is similar regardless of bed design and could be eliminated altogether in future designs. The heat load of the aluminum bed (Figure 27) is 2923 J/K. If the structural members are made of 304 stainless steel, the heat load of the system is 2086, a reduction of 29%. Mass is increased slightly (11%) however the volume consumed by the storage bed is 48% less. The benefit is clear to avoid aluminum for higher temperature structural components.

In addition to the bed re-design, if the entire system were designed as an integrated system, the fuel cell plate, and the backing plates reduced in mass or eliminated. If these two components were successfully eliminated, the system heat load would reduce from 7527 to 2086 J/K, a reduction of 72 percent! This would reduce the start up time required by the same amount from 2.51 hrs to 42 minutes without auxiliary heating.

Table 5. Energetic comparison of aluminum bed to the proposed stainless steel bed

Bed	Volume (cc)	Mass (kg)	Heat load per bed (J/K)
Aluminum	601	1.62	1462
Stainless steel	312	1.80	1043
% difference	Reduced **48%**	Increase **11%**	Reduced **29%**

These two design changes alone would reduce the heat load requirement by 72% and improve the startup time from 2.51 hours to 42 minutes. These are just two of many design optimizations that would be undertaken in follow-on work.

Intentionally left blank

5 Conclusion and future outlook

This project has successfully achieved its goals. Goals entailed demonstrating a proof of concept and entirely new approach to electrical power systems through the integration of a fuel cell with the hydrogen storage system. This is the first demonstration of any fuel cell running on hydrogen from alanates. The following objectives were undertaken and successfully completed:

1) ***Novel integrated approach to system thermal balance.***
   A unique engineering design based on integrating fuel cell stacks with hydride storage beds was used to develop an autonomous power delivery system.
   a) A total-system model was employed that incorporated fuel cell waste heat generation, composite-hydride desorption enthalpies, and system thermal conductivities to design a composite hydride system that was thermally matched with a high-temperature fuel cell.
   b) The results of the modeling were used to construct a proof-of-concept demonstration system.
   c) Experiments were performed. The high-temperature PEM fuel cell stack ran for more than an hour on hydrogen generated from the integrated alanate hydrogen storage system.

2) ***Modeling of heat and power generation for a typical demand cycle.***
   a) Modeling of the power demand cycles for typical applications was investigated as an initial step to determine an appropriate size of the demonstration system.
   b) A commercial fuel cell (1000 Watts) was purchased, tested and modeled.
   c) This modeling helped to define the operable pressure and temperature ranges of the hydrogen storage materials as well as the waste heat requirements to provide a steady generation of hydrogen.

3) ***Composite hydrides for cold start-up.***
   a) The Sandia data-base of the thermodynamic properties of classic hydrides was used to evaluate and select the best interstitial hydride to be used in combination with the alanates.
   b) Sorption rates were measured for the composite materials.
   c) This data combined with the thermodynamic data from the first task was incorporated into a system model to proportion the hydrides v.s. alanates. An optimum combination for this pilot system was determined to be a mass ratio of 1 interstitial hydride mass unit to 1.8 alanate mass units. This would provide you with 10 to 20 minutes of startup time.

4) ***Kinetics designed for rapid fill.***
The use of composite materials was evaluated for rapid fill as well as for cold start-up. Heat released from the low-temperature hydride increases the temperature of the system improving the kinetics of absorption of the high-temperature hydride. Experimental work confirmed our assumption that the recharging rate could be enhanced by using the two materials, but only when the materials are in separate gas handling sections of the same bed. This allows for the necessary benefit of heat transfer while maintaining control of the charge state of each material independently.

5) ***Hydrogen power milestone.***
The final product was a fully integrated set of the composite alanate-hydride beds and fuel cell stack.
   a) This system simulates a stand-alone "power-pack" for a variety of portable power applications.
   b) The test unit was designed and is available to test more advanced complex hydrides, amides and other hydrogen storage materials as they become available.
   c) An advanced version of this power-pack would be employed to demonstrate a number of different autonomous applications such as remote communications, robotics, single person transport, unmanned aircraft, etc.

Because this is an entirely new regime of temperatures, pressures and operating configuration for the fuel cell system as we know it, there is a great amount of learning, innovation and advancements in performance that will be generated from future work on this novel integrated system approach. We believe that a working experimental / demonstration platform is needed to address the many questions and state-of-the-art concepts that this new technology will generate. Sandia and its partners are in a unique position to move forward quickly with scientific and technical developments that this demonstration has proven possible.

Appendix: System drawings and schematics

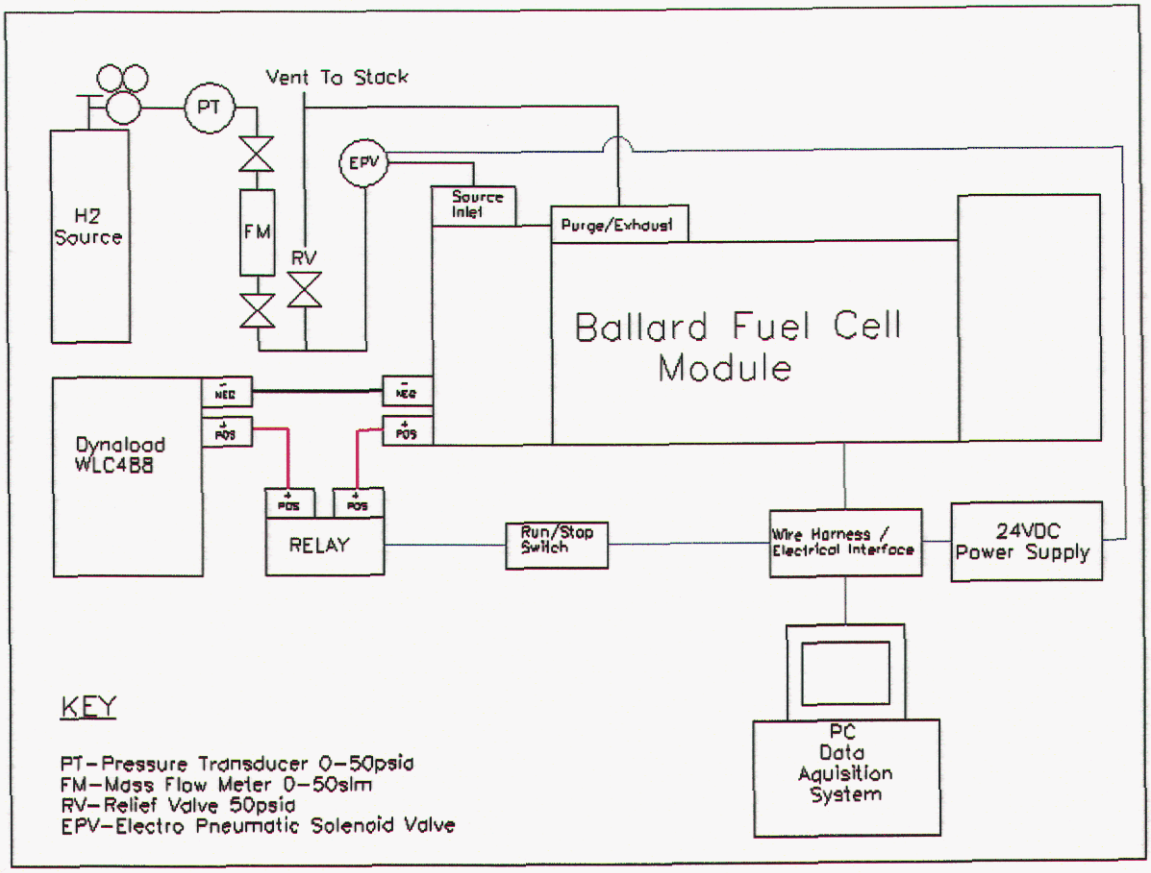

Figure 35. Schamatic of Nexa fuel cell characterization apparatus

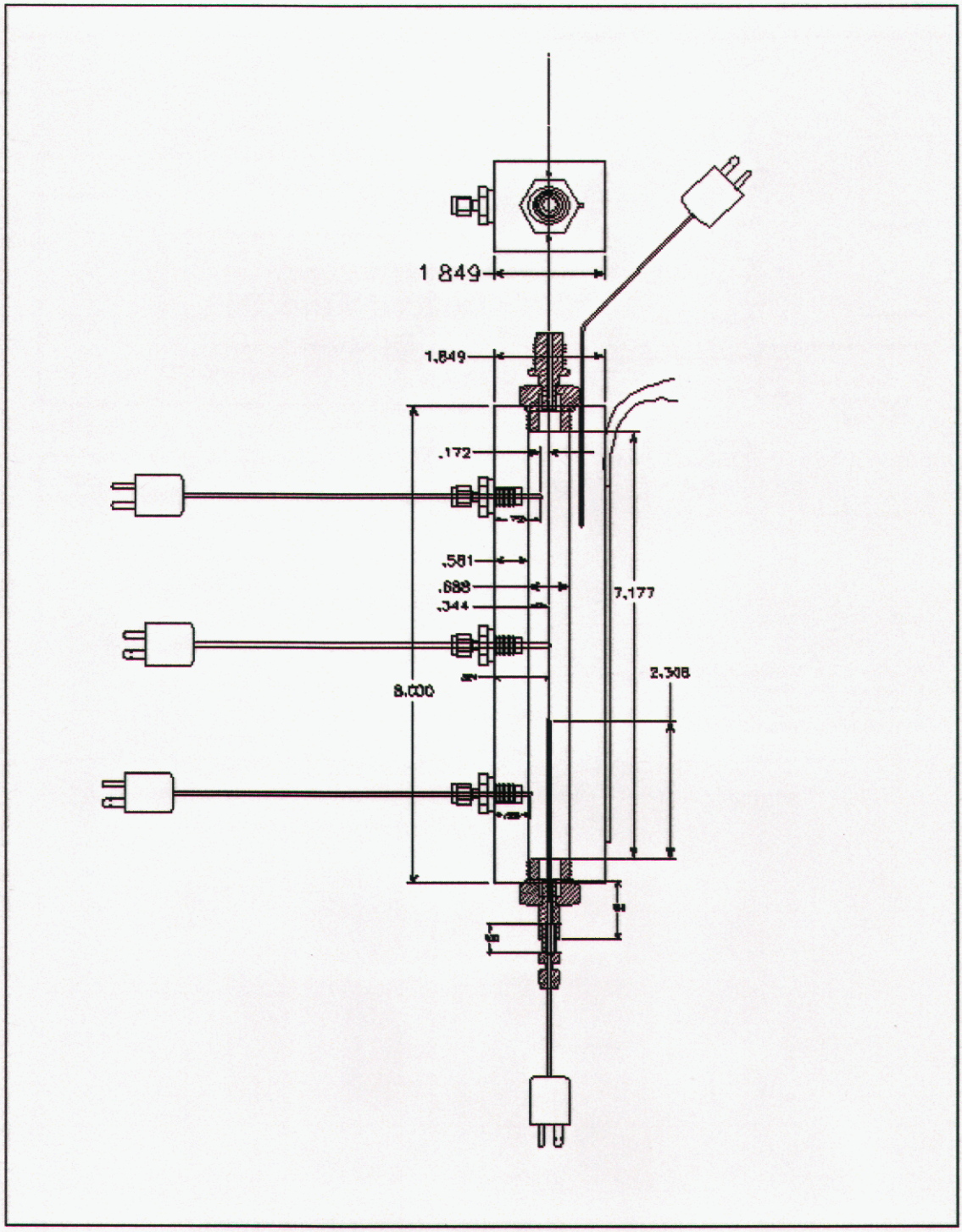

Figure 36. Drawing of single bed, all dimensions in inches

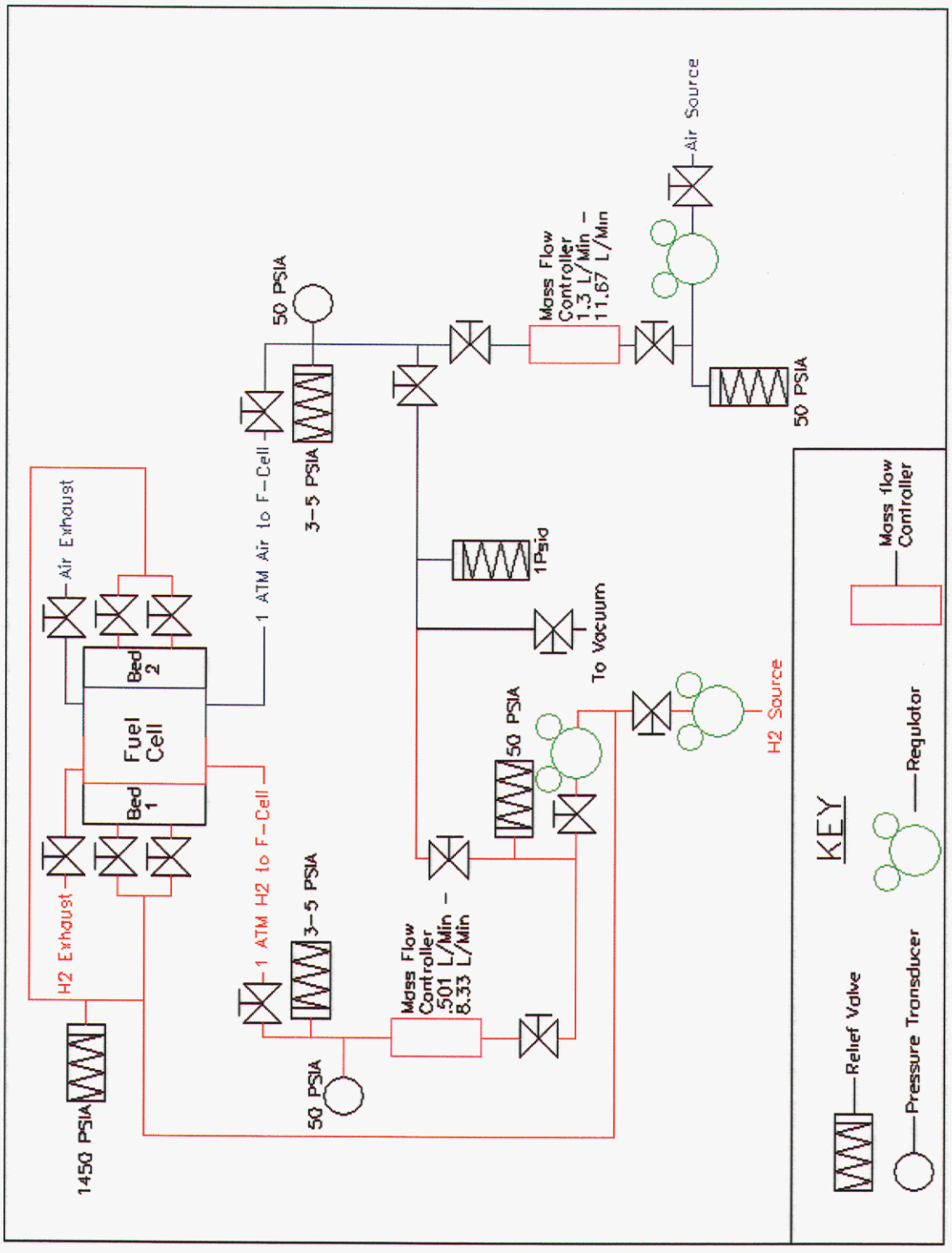

Figure 37. schematic of custom integrated hydrogen storage and fuel cell manifold

Intentionally left blank

References

1. "International Energy Annual," Energy Information Administration, U.S. Department of Energy (1995).
2. Miller, G. T., Living in the Environment, 7th ed., Wadsworth: Belmont, CA (1992).
3. Gates, D. M., Energy and Ecology, 1st ed., Sinauer Associates: Sunderland, MA (1985).
4. Taube, M., Materie, Energie and die Zukunft des Menschen, 1st ed., S. Hirzel, Wissenschaftliche Verlagsgesellschaft:Stuttgart (1988).
5. "Annual Energy Outlook," Energy Information Administration, U.S. Department of Energy (1997).
6. Reproduced from "Intermetallic Materials for Hydrogen Storage", Thesis N° 1217, K.J.Gross, Fribourg, 1998
7. Cannon, J. S., Harnessing Hydrogen, The Key to Sustainable Transportation, 1st ed., Inform: New York, NY (1995).
8. Winter, C. J., Nitsch, J., Wasserstoff als Energieträger, Technik, Systeme, Wirtschaft, 1st ed., Springer-Verlag: Berlin, Heidelberg, New York, Tokyo (1986).
9. Hennicke, P., Solarwasserstoff - Energieträger der Zunkunft, 1st ed., Birkhäuser Verlag, Bern, Basel
10. "Alternatives to Traditional Transportation Fuels: An Overview," Energy Information Administration, U.S. Depart-ment of Energy (1994).
11. Bogdanovic', B. and Schwickardi, M., J. Alloys and Compounds, 253 (1997) 1.
12. Gross, K.J., Thomas, G.J., and Sandrock, G., 2000. "Hydride development for hydrogen storage", in Proceedings U.S. DOE Hydrogen Program Review, NREL/CP-570-26938,452. Baltimore, MD.
13. Bogdanovic', B., Brand, R.A., Marjanovic', A., Schwikardi, M., and Tölle, J, J. Alloys and Compounds, 302 (2000) 36.
14. Gross, K.J., Guthrie, S., Takara, S., and Thomas, G.J., J. Alloys and Compounds, 297 (2000) 270.
15. Sandrock, G., Gross, K., Thomas, G.,Jensen, C., Meeker, D. and Takara, S., J. Alloys and Compounds 330-332 (2002) 696.
16. Jensen, C.M., Zidan, R.A., Mariels, N., Hee, A.G., and Hagen, C. Int. J. Hydrogen Energy, 24 (1999) 461.
17. Zidan, R.A., Takara, S., Hee, A.G., and Jensen, C.M. J. Alloys and Compounds, 285 (1999) 119.
18. Zaluska, A., Zaluski, L., and Strom-Olsen, J.O., J. Alloys and Compounds 298 (2000) 125.
19. Bogdanovic', B., and Sandrock, G., MRS Bulletin, 27(#9) (SEP 2002) 712.
20. Gross, K. J., Thomas, G. J., Majzoub, E. and Sandrock, G., (2001) "Light-weight Hydride Development ", in Proceedings U.S. DOE Hydrogen Program Review, NREL/CP-570-30535 San Ramon, CA.
21. Gross, K.J., Majzoub, E., Thomas, G.J., and Sandrock, G., (2002) "Hydride development for hydrogen storage", in Proceedings U.S. DOE Hydrogen Program Review, NREL/CP-610-32405. Golden, CO.

22. Majzoub, E.H. and Gross, K.J., "Titanium-halide catalyst-precursors in sodium aluminum hydrides", submitted to the proceedings of the International Symposium on Metal Hydrogen Systems, Annecy, France, Sept. 2-6, 2002, A. Percheron-Guegan editor.
23. U.S. Patent Appl, S.N. 10 / 066,375, (Jan. 29, 2002).
24. Fichtner,M., Fuhr, O., Kircher1, O. and Rothe, J. Nanotechnology 14 (2003) 778–785
25. B . Bogdanovic et al . / Journal of Alloys and Compounds 302 (2000) 36– 58
26. G. Sandrock, G. Thomas, IEA/DOE/SNL Hydride Databases, Internet URL http: / / hydpark.ca.sandia.gov
27. G.J. Thomas, S.E. Guthrie, K. Gross. Hydride Development For Hydrogen Storage, in: Proceedings of the 1999 U.S. DOE Hydrogen Program Review, NREL/CP-570-26938.
28. M.J. Craig, S. Dalin, S.R. Sesha, M. Keeley, P.N. Walter, K.K. Kristin, E. Michael, W. Zhaohui, G. Xue-Qin. Catalytically Enhanced Systems for Hydrogen Storage, in: Proceedings of the 1999 U.S. DOE Hydrogen Program Review, NREL/CP-610-32405.
29. Goodell, P.D.;Sandrock, G. D.; J. Less – Common Met. 73, (1980)
30. Reilly, J. J.; Wiswall, R. H.; Inorg. Chem. 13 (1974)
31. Reilly, J. J.; Chapter 2 in Hydrogen: Its Technology and Implications, CRC Press (1977), P. 13 (281)
32. D. E. Dedrick , M. P. Kanouff, B. C. Replogle, K. J. Gross. Thermal Properties Characterization of Sodium Alanates. Journal of Alloys and Compounds (accepted 4 August 2004) in print
33. E. Tsotsas, H. Martin, Chem. Eng. Process. 22 (1987) 19–37
34. Wang, Jim. Hydride Development for Hydrogen Storage. 2004 DOE Hydrogen Program Annual Review Proceedings.
35. Majzoub, EH; Somerday, BP; Goods, SH; Gross, KJ. Interactions between sodium aluminum hydride and candidate containment materials. International Conference on Hydrogen Effects on Material Behavior and Corrosion. September 22-26, 2002; Moran, WY
36. ASTM D 5334, Determination of Thermal Conductivity of Soil and Soft Rock by Thermal Needle Probe Procedure, (2000). Originally published as D 5334-5392.
37. Baumeister, Avallone, Baumeister. Mark's Standard Handbook for Mechanical Engineers. McGraw-Hill, 1978, pg 6-80.
38. Q. Li, R. He, J. Gao, J. O. Jensen and N. J. Bjerrum. The CO poisoning effect in polymer electrolyte membrane fuel cells operational at temperatures up to 200°C. J. Electrochem. Soc. 150 (12), A1599-A1605 (2003)
39. Q. Li, R. He, J. O. Jensen and N. J. Bjerrum. PBI-based polymer membranes for high temperature fuel cells – preparation, characterizations and fuel cell demonstrations. Fuel Cells 4 (3) 147-159 (2004)
40. Q. Li, R. He, J. O. Jensen and N. J. Bjerrum. Reviews: Approaches and recent development of polymer electrolyte membranes for fuel cells operational above 100 °C. Chemistry of Materials. 15, 4896-4915 (2003)

Distribution

16	MS9409	Daniel E. Dedrick
1	MS0123	Donna L. Chavez
3	MS9018	Central Technical File, 8945-1
1	MS0899	Technical Library, 9616
1	MS 9021	Classification Office, 8511 for Technical Library, MS 0899, 9616 DOE/OSTI via URL

Intentionally left blank